(Resubmission of E12-09-017 to Jefferson Lab PAC 37)

Transverse Momentum Dependence of Semi-Inclusive Pion and Kaon Production

December 1, 2010

A. Asaturyan, A. Mkrtchyan, H. Mkrtchyan (spokesperson), V. Tadevosyan, S. Zhamkochyan
Yerevan Physics Institute, Yerevan, Armenia

P. Bosted (spokesperson)
College of William and Mary, Williamsburg, VA 23187

H. Avagyan, S. Covrig, R. Ent (spokesperson), H.C. Fenker, D. Gaskell, M. Jones, D. Mack, J. Mei, Yi Qiang, B. Sawatzky, G. Smith, P. Solvignon, S. Wood
Jefferson Lab, Newport News, VA 23606

A. Bacchetta
Universitá di Pavia and INFN, Sez. di Pavia, Pavia, Italy

I. Albayrak, O. Ates, M.E. Christy, C.E. Keppel, M. Kohl, Y. Li, P. Monaghan, A. Pushpakumari, L. Tang, T. Walton, L. Yuan, L. Zhu
Hampton University, Hampton, VA 23668

G.M. Huber
University of Regina, Regina, Saskatchewan, Canada, S4S 0A2

D. Day, H. Baghdasaryan, N. Kalantarians
University of Virginia, Charlottesville, VA 22901

S. Danagoulian
North Carolina A & T State University, Greensboro, NC 27411

F.R. Wesselmann
Xavier University of Louisiana, New Orleans, LA

G. Niculescu, I. Niculescu
James Madison University, Harrisonburg, VA 22807

J. Dunne, D. Dutta
Mississippi State University, Mississippi, MS 39762

H. Gao, M. Huang, G. Laskaris, S. Malace, C. Peng, Q. J. Ye, Y. Zhang
Duke University/TUNL, Durham, NC 27708

T. Horn
Catholic University of America, Washington, DC 20064

Abstract

We propose to map the transverse momentum (P_t) dependence for semi-inclusive electroproduction of charged pions ($\pi^{\pm}$) and, simultaneously albeit with a factor of ten lower rates, kaons ($K^{\pm}$) from both proton and deuteron targets. The proposed measurements cover the range $0.2 < x < 0.5$, $2 < Q^2 < 5$ GeV^2, $0.3 < z < 0.5$, and $P_t < 0.5$ GeV.

The Hall C HMS spectrometer and the projected SHMS with its first-generation detector package will be used for electron and meson detection. The chosen setup of highly-focusing magnetic spectrometers with well-understood acceptances and redundant detector packages will allow precise determination of the P_t dependence of the *ratios* of π^+ to π^- cross sections. The proposed measurements correspond to a beam time request of 32 days, and assume a polarized electron beam to also include azimuthal asymmetry measurements, beam energies of 8.8 and (predominantly) 11.0 GeV, and varying beam currents of up to 75 μA.

The precision ratios will be combined with maps of the azimuthal asymmetries in semi-inclusive electroproduction of pions as approved for the unpolarized hydrogen target (E12-06-112, "Probing the Proton's Quark Dynamics in Semi-Inclusive Pion Production at 12 GeV") and envisioned for the unpolarized deuteron target (LOI12-07-103, LOI12-09-005 and a complementary CLAS12 proposal anticipated for PAC-38 emphasizing the deuteron/proton ratios and a complete (P_t, ϕ) coverage). In the context of a simple model, such combination of the proposed Hall C maps and the CLAS12 large-acceptance measurements constrain the initial transverse momentum widths of up and down quarks, and the transverse momentum widths of favored and unfavored fragmentation functions, respectively. We give a more detailed outline along the lines of this simple model below, using results of semi-inclusive pion electroroduction cross section measurements of the E00-108 experiment in Hall C, performed in 2003 with a 5.5 GeV beam energy, as an example. The latter also shows that although the physics proposed here benefits from its companion CLAS12 experimental program, it can stand on its own.

The proposed measurements emphasize the low P_t region, of scale Λ, as one-particle inclusive deep inelastic scattering off polarized and unpolarized nucleons have been the emphasis of recent theoretical studies. Such cross sections have been decomposed, using tree-level factorization, in terms of transverse-momentum-dependent parton distribution and fragmentation functions, for low transverse momentum of the scattered hadron [1].

Some of the kinematics benefit from overlap with the approved 12-GeV experiment E12-06-104 ("Measurement of the Ratio R = σ_L/σ_T in Semi-Inclusive Deep Inelastic Scattering").

As compared to the conditionally approved experiment E12-09-017, we have made the following changes:

- Recently, an NSF-MRI award was granted to augment the SHMS detection package with an aerogel detector, allowing simultaneous measurement of kaon cross sections.
- Polarized electron beam has been included as the default, to obtain azimuthal beam asymmetry measurements at low P_t.
- The kinematics and checkout are coordinated with the approved E12-06-104 experiment ("Measurement of the Ratio R = σ_L/σ_T in Semi-Inclusive Deep Inelastic Scattering") and the companion PAC-37 proposal for a "Precise Measurement of π^+/π^- Ratios in Semi-inclusive Deep Inelastic Scattering: Charge Symmetry Violating Quark Distributions" (a resubmittal of conditionally approved experiment E12-09-002). The collaborations have large overlap.

Contents

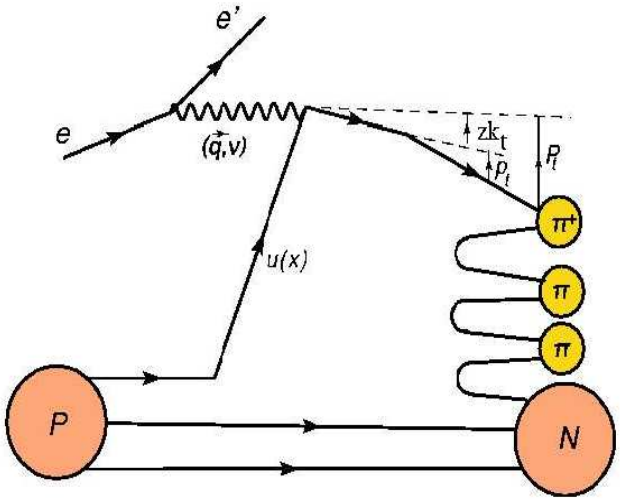

Figure 1: Schematic diagram of semi-inclusive pion electroproduction within a factorized QCD parton model at lowest order in α_s. Final transverse momenta of the detected pion $\vec{P}_t$ arises from convolving the struck quark transverse momenta $\vec{k}_t$ with the transverse momentum generated during fragmentation process $\vec{p}_t$.

1 Introduction

A central question in the understanding of nucleon structure is the orbital motion of partons. Much is known about the light-cone momentum fraction, x, and virtuality scale, Q^2, dependence of the up and down quark parton distribution functions (PDFs) in the nucleon. In contrast, very little is presently known about the dependence of these functions on their transverse momentum k_t. Simply based on the size of the nucleon in which the quarks are confined, one would expect characteristic transverse momenta of order a few hundred MeV, with larger values at small Bjorken x where the sea quarks dominate, and smaller values at high x where all of the quark momentum is longitudinal in the limit $x = 1$. Increasingly precise studies of the nucleon spin sum rule [2, 3, 4, 5] strongly suggest that the net spin carried by quarks and gluons is relatively small, and therefore the net orbital angular momentum must be significant. This in turn implies significant transverse momentum of quarks. Questions that naturally arise include: what is the flavor and helicity dependence of the transverse motion of quarks and gluons, and can these be modeled theoretically and measured experimentally?

The process of semi-inclusive deep-inelastic lepton scattering (SIDIS), $lN \to lhX$ has been shown to factorize [6], in the high energy limit, into lepton-quark scattering followed by quark hadronization. Ideally, one could then directly measure the transverse momentum dependence of the quark distribution functions $q(x, k_t)$ by detecting all particles produced in the hadronization process of the struck quark. This idealization is complicated in practice, as measurements can in principle never unambiguously state a hadron originates from the quark struck in the hard scattering process.

Nonetheless, in the present experiment we aim for kinematics to largely fulfill the mentioned idealization. We will detect only a single hadronization product: a charged pion (or kaon)

carrying an energy fraction z of the available energy. The probability of producing a pion with a transverse momentum P_t relative to the virtual photon ($\vec{q}$) direction is described by a convolution of the quark distribution functions and p_t-dependent fragmentation functions $D^+(z, p_t)$ and $D^-(z, p_t)$, where p_t is the transverse momentum of the pion relative to the quark direction, with the imposed condition [7] $\vec{P}_t = z\vec{k}_t + \vec{p}_t$ (see Fig. 1). The "favored" and "unfavored" functions $D^+(z, p_t)$ and $D^-(z, p_t)$ refer to the case where the produced pion contains the same flavor as the struck quark or not. "Soft" non-perturbative processes are expected [7] to generate relatively small values of p_t with an approximately Gaussian distributions in p_t. Hard QCD processes are expected to generate large non-Gaussian tails for $p_t > 1$ GeV, and probably do not play a major role in the interpretation of the present experiment, for which the total transverse momentum $P_t < 0.5$ GeV. The assumption that the fragmentation functions do not depend on quark flavor (for example $D^+(z, p_t)$ applies equally well to $u \to \pi^+$ and $d \to \pi^-$) in principle allows the k_t widths of up and down quarks to be distinguished, under the assumption that the contribution of sea quarks can be neglected at sufficiently large x. In the present experiment, the use of both proton and deuteron targets (the latter with a higher d quark content than the former) and the detection of both π^+ and π^- then permits a first dedicated study of this problem.

2 Physics

The possibility of a study of the k_t widths of up and down quarks under the main assumption that the fragmentation functions do not depend on quark flavor (and several other assumptions, see below) was first indicated following the results of the E00-108 experiment in Hall C at Jefferson Lab [8]. In this Section, we will further describe the findings of this E00-108 experiment, paving the road for a dedicated 12-GeV experiment, outlined in the later Sections.

2.1 The E00-108 Experiment

The E00-108 experiment used the Short Orbit (SOS) and High Momentum (HMS) spectrometers in Hall C at Jefferson Lab to detect final state electrons and pions, respectively. An electron beam with energy of 5.5 GeV and currents ranging between 20 and 60 μA were provided by the CEBAF accelerator. Incident electrons were scattered from 4-cm-long liquid hydrogen or deuterium targets. The E00-108 experiment consisted of three parts: i) at a fixed electron kinematics of $(x, Q^2) = (0.32,\ 2.30\ \text{GeV}^2)$, z was varied from 0.3 to 1, with nearly uniform coverage in the pion azimuthal angle, ϕ, around the virtual photon direction, but at a small average P_t of 0.05 GeV; ii) for $z = 0.55$, x was varied from 0.2 to 0.5 (with a corresponding variation in Q^2, from 2 to 4 GeV^2), keeping the pion centered on the virtual photon direction (and again average P_t of 0.05 GeV); iii) for $(x, Q^2) = (0.32,\ 2.30\ \text{GeV}^2)$, z near 0.55, P_t was scanned from 0 to 0.4 GeV by increasing the HMS angle (with average ϕ near 180 degrees). The ϕ distribution as a function of P_t is shown for all three data sets combined in Fig. 2. The virtual photon-nucleon invariant mass W, was always larger than 2.1 GeV (typically 2.4 GeV), corresponding to the traditional deep inelastic region for inclusive scattering.

At lower virtual photon energy and/or mass scales, the factorization ansatz is expected to break down, due to the effects of final state interactions, resonant nucleon excitations, and higher twist contributions [9]. In particular, in the present experiment the residual invariant

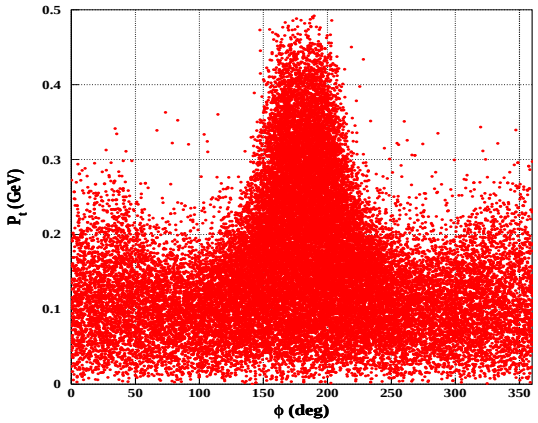

Figure 2: P_t distribution of data from this experiment as a function of ϕ.

mass M_x of the undetected particles (see Fig. 1) ranges from about 1 to 2 GeV (inversely correlated with z), spanning the mass region traditionally associated with significant baryon resonance excitation. The extent to which this situation leads to a break-down of factorization was studied in our previous paper [10]. It was found that good agreement with expectations based on higher energy data was achieved for $z < 0.7$, approximately corresponding to $M_x > 1.5$ GeV. The ratio of total up to down quark distributions $u(x)/d(x)$ extracted from ratios of cross sections, as well as the ratio of valence-only up to down ratios $u_v(x)/d_v(x)$, were also found to be reasonably compatible with higher energy extractions, provided $z < 0.7$. This issue will be addressed further for the P_t-scan data below. Finally, the ratio of unfavored to favored fragmentation functions $D^-(z)/D^+(z)$ (from the π^-/π^+ ratios on the deuteron) was found to be consistent with extractions from other experiments. All of these studies were done with the z-scan and x-scan data, for which the average P_t was small (< 0.1 GeV), and the average value of $\cos(\phi)$ was close to zero.

2.2 Transverse momenta and azimuthal angles

In the E00-108 analysis, and in this proposal, we focus on the P_t dependence, with the goal of searching for a possible flavor dependence to the quark distribution functions and/or fragmentation functions. Since the average value of $\cos(\phi)$ in the E00-108 experiment is correlated with P_t (approaching -1 for the largest P_t value of 0.45 GeV, see Fig. 2), we first study the limited data available from the E00-108 experiment on the ϕ dependence, which must be an even function since neither the beam nor the target were polarized. We parameterize [11] the data for each target and pion flavor according to:

$$\frac{d\sigma_{ee'\pi x}}{d\sigma_{ee'x}} = \frac{dN}{dz}\, b\, \exp(-bP_t^2)\, \frac{1 + A\cos\phi + B\cos(2\phi)}{2\pi} \tag{1}$$

where the parameters $A(x, Q^2, z, P_t)$ and $B(x, Q^2, z, P_t)$ are a measure of the relative importance of the interference terms σ_{LT} and σ_{TT}, respectively [12]. The assumed Gaussian P_t dependence

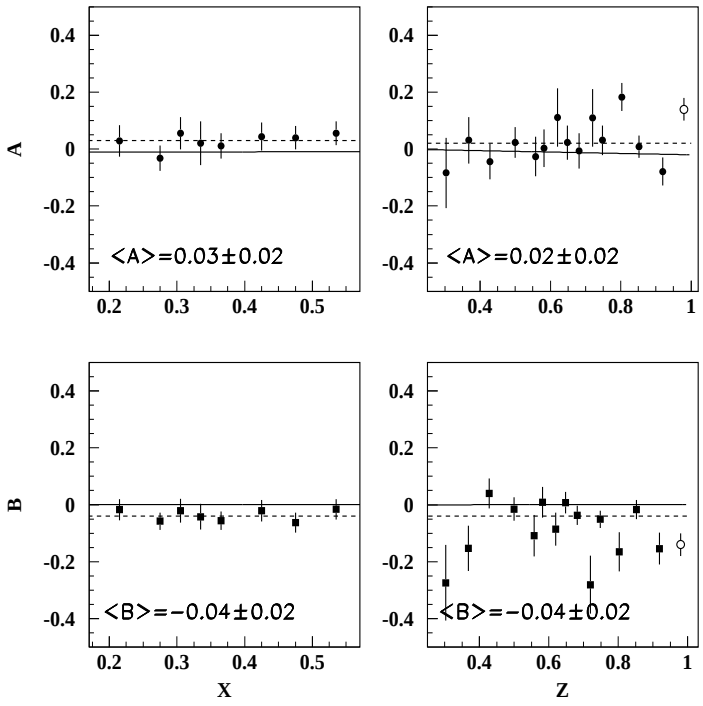

Figure 3: The parameters A and B [the relative coefficients of the $\cos\phi$ (σ_{LT}) and $\cos 2\phi$ (σ_{TT}) terms] averaged over π^+ and π^- detected from proton and deuteron targets, as a function of x at $\langle z\rangle$=0.55 (left), and as a function of z at $\langle x\rangle$=0.32 (right). The data form the experiment E00-108 [10, 8]. The average value of transverse momentum ($\langle|P_t|\rangle$) is ∼0.05 GeV. The dashed lines indicate the weighted averages for $z < 0.7$, which are also enumerated in each panel. Errors indicated include only statistical contributions. Systematic errors are highly correlated from point to point, and are estimated at 0.03 on both A and B. The open symbols are from exclusive pion production (see text). The solid lines are theoretical predictions [13].

(with exponential slope b) is an effective parameterization that seems to describe the data adequately for use in making radiative and bin-centering corrections. We use this model for studying the ϕ dependence, then return to a more detailed study of the P_t dependence in the context of a simple model that incorporates a different P_t dependence for each struck quark and produced hadron flavor.

For each kinematic point in the x and z scans (average $P_t = 0.05$ GeV, with a maximum $P_t \sim 0.4$ GeV), we extracted A and B and found no statistically significant difference between the results for π^+ or π^-, or proton or deuteron targets. We therefore combined all four cases together, and present the results in Fig. 3.

Systematic errors (not shown in the figure) are approximately 0.03 on both A and B and are highly correlated from point to point. Taking the systematic errors into account, the values of A and B are close to zero, for all values of x studied, and for values of $z < 0.7$, where our previous studies showed a good consistency with factorization. The small values of A and B are also consistent with the expectations based on kinematic shifts due to parton motion as described by Cahn [13] (shown as the solid curves on the figures) and Levelt-Mulders [14]. These effects are

proportional to P_t for A, and P_t^2 for B respectively [13, 14, 15, 16], so are suppressed at low P_t. More specifically, using the assumption that the average quark and fragmentation transverse momentum distribution widths are equal, the Cahn [13] asymmetries are given by

$$A = -\gamma(2 < P_t > /Q)(2-y)\sqrt{1-y}/[1+(1-y)^2], \quad (2)$$

$$B = -\gamma^2(2 < P_t^2 > /Q^2)(1-y)/[1+(1-y)^2], \quad (3)$$

where $\gamma = z^2/(1+z^2)$, $y = \nu/E$, ν is the virtual photon energy, and E is the beam energy, yielding $A = -0.01$ and $B = -0.0002$ for $z = 0.55$. The more recent treatment of Ref. [7] also gives results for A and B which are very close to zero (especially for B). Other possible higher twist contributions will also be proportional to powers of $P_t/\sqrt{(Q^2)}$ [17, 18], and therefore suppressed at our lower average values of P_t and P_t^2. Specifically, the twist-2 Boer-Mulders [19] contribution to B is essentially zero in the models of Ref. [19, 20].

For the kinematic of present proposal, for π^+ the value of B is positive and could change approximately linear with x, z and P_t from $\sim$0.002 to $\sim$0.02. For π^- it is expected negative and the dependences are much weaker. (See Fig.6 and Fig.7 in Ref. [21]).

In contrast, the longitudinal-transverse and transverse-transverse coefficients A and B are much larger in exclusive pion production ($M_x = M$, where M is the nucleon mass) than those predicted for SIDIS. This is evidenced by our extracted average values for exclusive $\pi^\pm$ electroproduction on deuteron and for π^+ on proton, shown as the open symbols near $z = 0.98$ in Fig. 3. This underlines the importance of accounting for the radiative tail from exclusive production, which in our analysis was done using the computer code EXCLURAD [22] together with a reasonable model of exclusive pion electroproduction. The corrections where checked with the Hall C simulation package SIMC, which treats radiative corrections in the energy and angle peaking approximation [23].

2.3 Transverse Momentum P_t Dependence

We now turn to the study of the P_t scan data from the E00-108 experiment. We used the cross section model from our previous paper [10] to describe the Q^2 dependence of the data (needed because P_t and Q^2 are somewhat correlated), and extracted cross sections at fixed Q^2 averaged over ϕ. The corrections for Q^2 dependence did not distinguish between targets or pion flavor. Relatively small corrections (typically a few percent) for radiative effects (including the tails from exclusive pion production) and diffractive ρ production were made [10] for each case individually. The systematic error on these corrections is estimated to be approximately 2%. The normalization errors due to target thickness, computer and electronic dead time, beam charge measurement, beam energy, and spectrometer kinematics combine to approximately 2% overall, and 1% from case to case. The overall error due to spectrometer acceptance is estimated to be 3%, but $< 1\%$ from case to case because targets were exchanged frequently, as was the spectrometer polarity. Since the acceptance as defined by the focusing magnetic spectrometer setup is essentially identical for all four combinations, the ratios of cross sections are dominated by statistical rather than systematic errors.

The extracted cross sections are shown in Fig. 4. The acceptance-averaged values of $\cos(\phi)$ range from -0.3 at low P_t to nearly -1 at higher P_t, while the average values of $\cos(2\phi)$ approaches

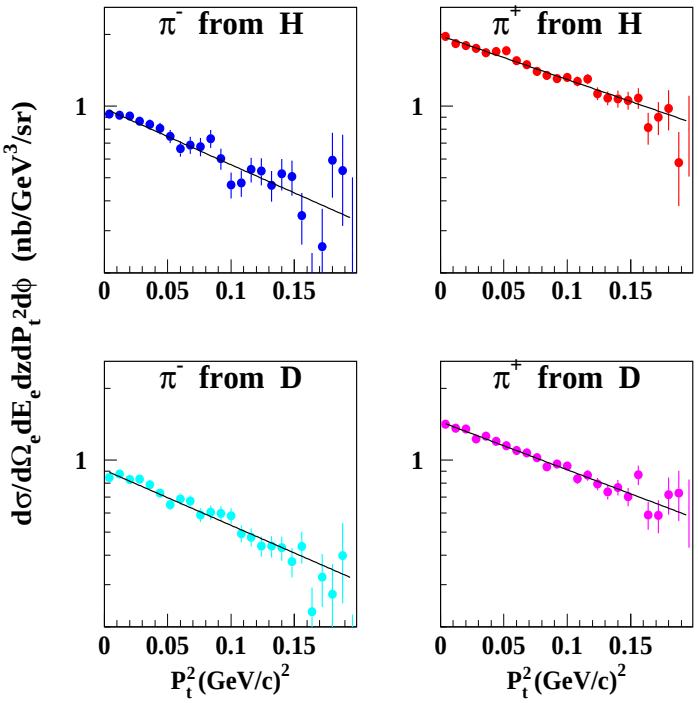

Figure 4: The P_t^2 dependence of differential cross-sections per nucleon for $\pi^{\pm}$ production on hydrogen (H) and deuterium (D) targets at $\langle z\rangle$=0.55 and $\langle x\rangle$=0.32. The solid lines are exponential fits. The error bars are statistical only. Systematic errors are typically 4% (relative, see text in Ref. [8] for details). The average value of cos(ϕ) varies with P_t^2.

1 at high P_t (See Fig. 2). Fig. 4 shows that the P_t-dependence for π^+ and π^- are very similar to each other for each target.

A recent study [24] analyzed these data in combination with the CLAS data [25], and concluded that in the kinematics similar to the CLAS data, the Hall C data could be relatively well described by a Gaussian model with average transverse momentum width of 0.24 GeV^2. The good description of the $\pi^{\pm}$ cross sections from different targets was argued to indicate that the assumption of flavor-independent Gaussian widths for both the transverse widths of quark and fragmentation functions was reasonable, in the valence-x region for $z = 0.55$.

If taken as standalone data, a careful examination of Fig. 4 shows however that the P_t-dependent slopes for the deuteron target are somewhat smaller than those for the proton. For a more quantitative understanding of the possible implications of this, we studied the data in the context of a simple model in which the P_t dependence is described in terms of two Gaussian distributions for each case. Following Ref. [7], we assume that the widths of quark and fragmentation functions are Gaussian in k_t and p_t, respectively, and that the convolution of these distributions combines quadratically. The main difference from Ref. [7] is that we allow separate widths for up and down quarks, and separate widths for favored and unfavored fragmentation functions. The widths of the up and down distributions are given by μ_u and μ_d, respectively, and the favored (unfavored) fragmentation widths are given by μ_+ (μ_-). Following Cahn [13] and more recent studies [7], we assume that only the fraction z of the quark transverse momentum

contributes to the pion transverse momentum (see Fig. 1). We assume further that sea quarks are negligible (typical global fits show less than 10% contributions at $x = 0.3$). To make the problem tractable, we take only the leading order terms in (k_t/Q), which was shown to be a reasonable approximation for small to moderate P_t in Ref. [7]. The simple model can then be written as:

$$\begin{aligned}
\sigma_p^{\pi^+}(P_t) &= C[4c_1(P_t)e^{-b_u^+ P_t^2} + (d/u)(D^-/D^+)c_2(P_t)e^{-b_d^- P_t^2}] \\
\sigma_p^{\pi^-}(P_t) &= C[4(D^-/D^+)c_3(P_t)e^{-b_u^- P_t^2} + (d/u)c_4(P_t)e^{-b_d^+ P_t^2}] \\
\sigma_n^{\pi^+}(P_t) &= C[4(d/u)c_4(P_t)e^{-b_d^+ P_t^2} + (D^-/D^+)c_3(P_t)e^{-b_u^- P_t^2}] \\
\sigma_n^{\pi^-}(P_t) &= C[4(d/u)(D^-/D^+)c_2(P_t)e^{-b_d^- P_t^2} + c_1(P_t)e^{-b_u^+ P_t^2}]
\end{aligned} \tag{4}$$

where C is an arbitrary normalization factor, and the inverse of the total widths for each combination of quark flavor and fragmentation function are given by

$$\begin{aligned}
b_u^\pm &= (z^2\mu_u^2 + \mu_\pm^2)^{-1} \\
b_d^\pm &= (z^2\mu_d^2 + \mu_\pm^2)^{-1}
\end{aligned} \tag{5}$$

and we assume $\sigma_d = (\sigma_p + \sigma_n)/2$. The Cahn effect [13, 7] is taken into account through the terms:

$$\begin{aligned}
c_1(P_t) &= 1. + c_0(P_t, <\cos(\phi)>)\mu_u^2 b_u^+ \\
c_2(P_t) &= 1. + c_0(P_t, <\cos(\phi)>)\mu_d^2 b_d^- \\
c_3(P_t) &= 1. + c_0(P_t, <\cos(\phi)>)\mu_u^2 b_u^- \\
c_4(P_t) &= 1. + c_0(P_t, <\cos(\phi)>)\mu_d^2 b_d^+ \\
c_0(P_t, <\cos(\phi)>) &= \frac{4z(2-y)\sqrt{1-y}}{\sqrt{Q^2}[1+(1-y)^2]}\sqrt{P_t^2} <\cos(\phi)> .
\end{aligned} \tag{6}$$

We fit for the four widths (μ_u, μ_d, μ_+, and μ_-), C, and the ratios D^-/D^+ and d/u, where the fragmentation ratio is understood to represent the data-averaged value at $z = 0.55$, and the quark distribution ratio is understood to represent the average value at $x = 0.3$. The fit describes the data reasonably well ($\chi^2 = 68$ for 73 degrees of freedom), and finds the ratio $d/u = 0.37 \pm 0.02$, close to the value given by the LO GRV98 fit [26] for valence quarks (about 0.40). The fit also gives a reasonable value for the ratio $D^-/D^+ = 0.42 \pm 0.01$ (a fit to HERMES results [27], $D^-/D^+ = 1/(1+z)^2$, predicts 0.42 at $z = 0.55$). Both d/u and D^-/D^+ are largely uncorrelated with other fit parameters.

Since the data are at fixed z, the main contributions that distinguishes large fragmentation widths from large quark widths are the ϕ-dependence Cahn-effect c_i terms. While there is a significant inverse correlation between the two most important quark and fragmentation widths, (μ_u and μ_+, respectively), the fit indicates a preference for μ_u to be smaller than μ_+ as shown in Fig. 5a. The fit also indicates a preference for μ_d to be smaller than μ_- as shown in Fig. 5b. So, in both cases, fragmentation widths appear to somewhat dominate over quark widths, within our simple model.

The fit parameters indicate a non-zero k_t width squared for u quarks ($\mu_u^2 = 0.09 \pm 0.03$ (GeV/c)^2), but a d-quark width squared that is consistent with zero ($\mu_d^2 = 0 \pm 0.05$ (GeV/c)^2), as illustrated in Fig. 5c. The results are consistent with a di-quark model [28] in which the d quarks are only found in an axial di-quark, while the u quarks are predominantly found in a scalar di-quark. We plotted the results with equal axial and scalar di-quarks masses (M_a

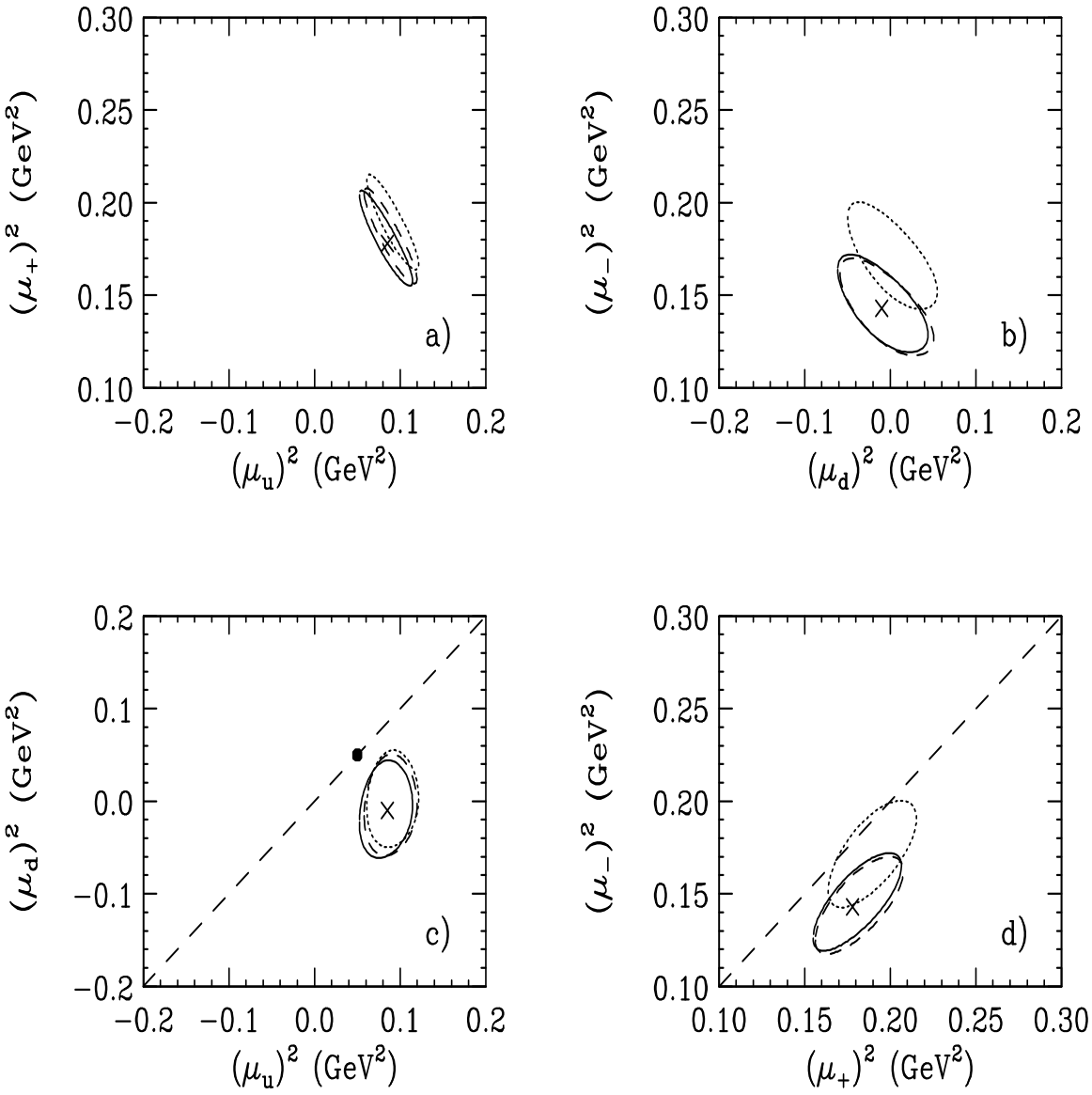

Figure 5: Fit parameters (crosses) and one-standard-deviation contours (continuous ellipses) from the seven-parameter fit to the data shown in Fig. 4: a) u quark width squared μ_u^2 versus favored fragmentation width squared μ_+^2; b) μ_d^2 versus μ_-^2; c) μ_u^2 versus μ_d^2; d) μ_-^2 vs μ_+^2. The dashed and dotted contours are for the case of no diffractive ρ subtraction and a 30% reduction in the size of the exclusive radiative tail subtraction, respectively. The large dot near the middle of panel c is from a di-quark model [28]. The dashed straight lines in panels c and d indicate $\mu_u^2 = \mu_d^2$ and $\mu_-^2 = \mu_+^2$, respectively.

and M_s) of 0.6 GeV/c; picking $M_a < M_s$ results in $\mu_d^2 < \mu_u^2$, and visa verse, with the average remaining near 0.06 $(\mathrm{GeV/c})^2$.

Using the fit parameters, we find the magnitude of the $\cos(\phi)$ term A at $P_t = 0.4$ GeV/c to be about -0.15 ± 0.05 for all four cases. These results are similar in sign and magnitude to those found in the HERMES experiment [29].

We find that the fragmentation widths μ_+ and μ_- are correlated, as illustrated in Fig. 5d, although the allowed range is not large, and the central values ($\mu_+^2 = 0.18 \pm 0.03$ $(\mathrm{GeV/c})^2$ and $\mu_-^2 = 0.14 \pm 0.03$ $(\mathrm{GeV/c})^2$) are in reasonable agreement with both each other and also the flavor-averaged value of 0.20 GeV^2 found in Ref. [7]. While there is a slight tendency for the favored width to be larger than the unfavored one, a reasonable fit can be obtained setting the widths equal to each other ($\chi^2 = 71$ for 74 d.f., $\mu_+^2 = \mu_-^2 = 0.17 \pm 0.03$ $(\mathrm{GeV/c})^2$). Taking into account the systematic uncertainties from the diffractive ρ and exclusive tail subtractions, the favored and un-favored widths are consistent with each other.

To estimate the effect of experimental systematic uncertainties on our fit results, we repeated the fits with: no diffractive ρ subtraction; 30% smaller exclusive radiative tail subtraction; relative target thickness changed by 1%; and difference in π^+ and π^- absorption changed by 1%. The last three changes had a negligible effect compared to statistical errors. The first change mainly affected μ_-^2, shifting it to a more positive value by almost the size of the statistical error, as shown in Fig. 5. We found no significant change to the fit parameters upon adding to μ_u^2 and μ_d^2 an average nucleon transverse momentum squared of 0.001 $(\mathrm{GeV/c})^2$ (evaluated using the Paris wave function [30]) for the deuteron model.

2.4 Summary of E00-108 Findings

In summary, E00-108 measured semi-inclusive electroproduction of charged pions ($\pi^\pm$) from both proton and deuteron targets, using 5.5 GeV energy electrons at Jefferson Lab. E00-108 finds the azimuthal dependence to be small, compared to exclusive pion electroproduction, and consistent with theoretical expectations [13, 7].

In the context of a simple model with only valence quarks and only two fragmentation functions, E00-108 finds the (valence) quark k_t widths to be smaller than the (favored and unfavored) fragmentation p_t widths. The favored and unfavored fragmentation widths are found to be correlated, and the central values are found to be in reasonable agreement with both each other and the flavor-averaged value of 0.20 GeV^2 of Anselmino *et al.* [7].

All of the above fit results can only be considered as suggestive at best, due to the limited kinematic range covered, the somewhat low u/d ratio that we find, and the very simple model assumptions described above. Many of these limitations could be removed with future experiments covering a wide range of Q^2 (to resolve additional higher twist contributions), full coverage in ϕ, a larger range of P_t, a wide range in z (to distinguish quark width terms, which is weighted by powers of z, from fragmentation widths, which likely vary slowly with z), and including the π^0 final state for an additional consistency check (particularly on the assumption that only two fragmentation functions are needed for charged pions from valence quarks). These goals should be attainable with this proposed 12-GeV experiment, emphasizing semi-inclusive charged-pion electroproduction, in combination with the approved and planned experimental 12-GeV program with the CLAS12 detector (where one would also more naturally include the π^0 final state). The data foreseen with this proposed experiment should then provide potential

crucial information on how hadron transverse momentum in SIDIS is split between fragmentation and intrinsic quark contributions.

3 Experiment

The proposed experiment will use the HMS and SHMS magnetic spectrometers for coincidence measurement of scattered electrons and charged pions from the semi-inclusive electroproduction reaction $(e, e'\pi^{\pm})$X. HMS will be used to measure the scattered electrons, whereas SHMS, with its most forward angle of 5.5°, will detect the electroproduced pions. The HMS can reach scattering angles down to 10.5°, and sub-tends a scattering angle acceptance of about 3° (for a point source). The minimum *separation* angle of HMS and SHMS is 17.5°, which prevents the HMS and SHMS from both being at their most forward angle simultaneously.

The experiment will use a beam energy of 11 GeV to map a region in Bjorken x between 0.2 and 0.5, in z between 0.3 and 0.5, and in θ_{pq} to cover a range in P_t up to 0.5 GeV. To better constrain the possible (x, z) entanglement, we plan to measure over a range in Q^2 for *fixed* value of $x = 0.30$, while still varying z between 0.3 and 0.5 (or 0.25 and 0.6 or so, within the spectrometer momentum acceptances). To cover a wide range in Q^2, from 1.8 to 4.5 GeV^2, a limited time of 8.8 GeV beam energy running is required. An 8.8 GeV beam energy constitutes the same base Linac energy of 2.2 GeV/pass, but at four passes only.

The residual invariant mass M_x of the undetected particle ranges from 1.7 to 2.8 GeV, inversely correlated with z. In the E00-108 experiment, as mentioned above and reported in [10], good agreement with expectations based on a high-energy assumption of factorization in terms of structure and fragmentation functions was achieved for $z < 0.7$, approximately corresponding to $M_x > 1.5$ GeV. We have used the larger kinematic flexibility utilizing an 11-GeV beam energy (as compared to the 5.5 GeV beam energy of E00-108) to be comfortably within these ranges, and obtaining a somewhat improved, more uniform, coverage in azimuthal angle ϕ.

We contemplated substituting the highly-focusing magnetic spectrometer functioning as electron arm with a larger-acceptance non-magnetic detector, or a detector with a single magnetic field, but decided against this. The magnetic spectrometer setup used allows access to small electron angles, which compensates largely for the reduction in acceptance. In addition, an alternate setup often reduces the allowable beam current even more to limit the Moller flux at forward angles. Lastly, at larger electron scattering angles the need for good electron identification becomes more important, related to the larger π/e ratios and the increased possibility for (π, π) coincidences. Our goal is for this experiment to provide precision constraints on ratios of charged-pion electroproduction and their transverse momentum dependence. Lastly, the requested beam time could be reduced by 15% ($\approx$ 5 days) utilizing overlap of kinematics and overhead with the approved E12-06-104 experiment [31]. We note that in addition the conditionally-approved companion experiment E12-09-002, which is also coordinated for maximum overlap of kinematics and checkout.

We intend to perform all measurements on 10 cm long hydrogen and deuterium targets, apart from the necessary Al "dummy" measurements for target wall subtraction. The beam currents vary to constrain the maximum singles rate in the hadron spectrometer (SHMS) to less than 700 kHz. This maximum rate has been chosen to minimize the uncertainty in tracking efficiency and detector efficiencies. The target density will be monitored by pressure and temperature

measurements. We expect negligible change in target densities with the fast raster systems already in place: less than 0.5% density changes at 50 μA, for a raster size of 2×2 mm^2.

We plan to use the base equipment detector packages for HMS and SHMS, augmented with an aerogel detector for kaon/proton separation. The latter would allow us to also independently map the kaon yields, albeit with about an order of magnitude less rate. This would still render yield greater than 1,000 counts per setting.

4 Proposed Measurements

We propose to map the transverse momentum dependence of charged pion $\pi^{\pm}$ electroproduction off hydrogen and deuterium targets, at small transverse momentum (scale $P_t \approx \Lambda$), where the cross sections have been recently calculated at tree level in terms of transverse-momentum dependent parton distribution and fragmentation functions [1]. Recent measurements hint at a possibility to extract information on the average transverse momentum of (unpolarized) valence quarks from such studies. Regardless, the measurements are to date hardly constrained.

4.1 Choice of Kinematics

We propose to map the x, z, and P_t dependence of the semi-inclusive pion electroproduction process off both proton and deuteron targets by variation of angle and momentum of electron arm (HMS) and hadron arm (SHMS) (see Table 1-7). We will measure the semi-inclusive charged-pion electroproduction yields over the range in z and θ_{pq} at:

1. $(x,\ Q^2) = (0.20,\ 2.0\ \text{GeV}^2)$, (kinematics I).
2. $(x,\ Q^2) = (0.30,\ 3.0\ \text{GeV}^2)$, (kinematics II).
3. $(x,\ Q^2) = (0.40,\ 4.0\ \text{GeV}^2)$, (kinematics III).
4. $(x,\ Q^2) = (0.50,\ 5.0\ \text{GeV}^2)$, (kinematics IV).
5. $(x,\ Q^2) = (0.30,\ 1.8\ \text{GeV}^2)$, (kinematics V).
6. $(x,\ Q^2) = (0.30,\ 4.5\ \text{GeV}^2)$, (kinematics VI).

In all cases, we have made sure that the laboratory angle of SHMS is at least 5.5°, and the laboratory angle of HMS at least 10.5°. For the first kinematics, at $(x,\ Q^2) = (0.20,\ 2.00\ \text{GeV}^2)$, we will park the HMS at 10.5° and benefit from the ≈3° angular acceptance of HMS to cover the nominal 10.27° scattering angle. The spectrometer momentum settings are well within the allowable ranges for the HMS and SHMS, and we assumed a 2.5° step in θ_{pq} to cover a large P_t range, up to 0.5 GeV, with sufficient overlap between the various settings. See Figures 6 to illustrate the (P_t, ϕ) coverage for the various kinematics.

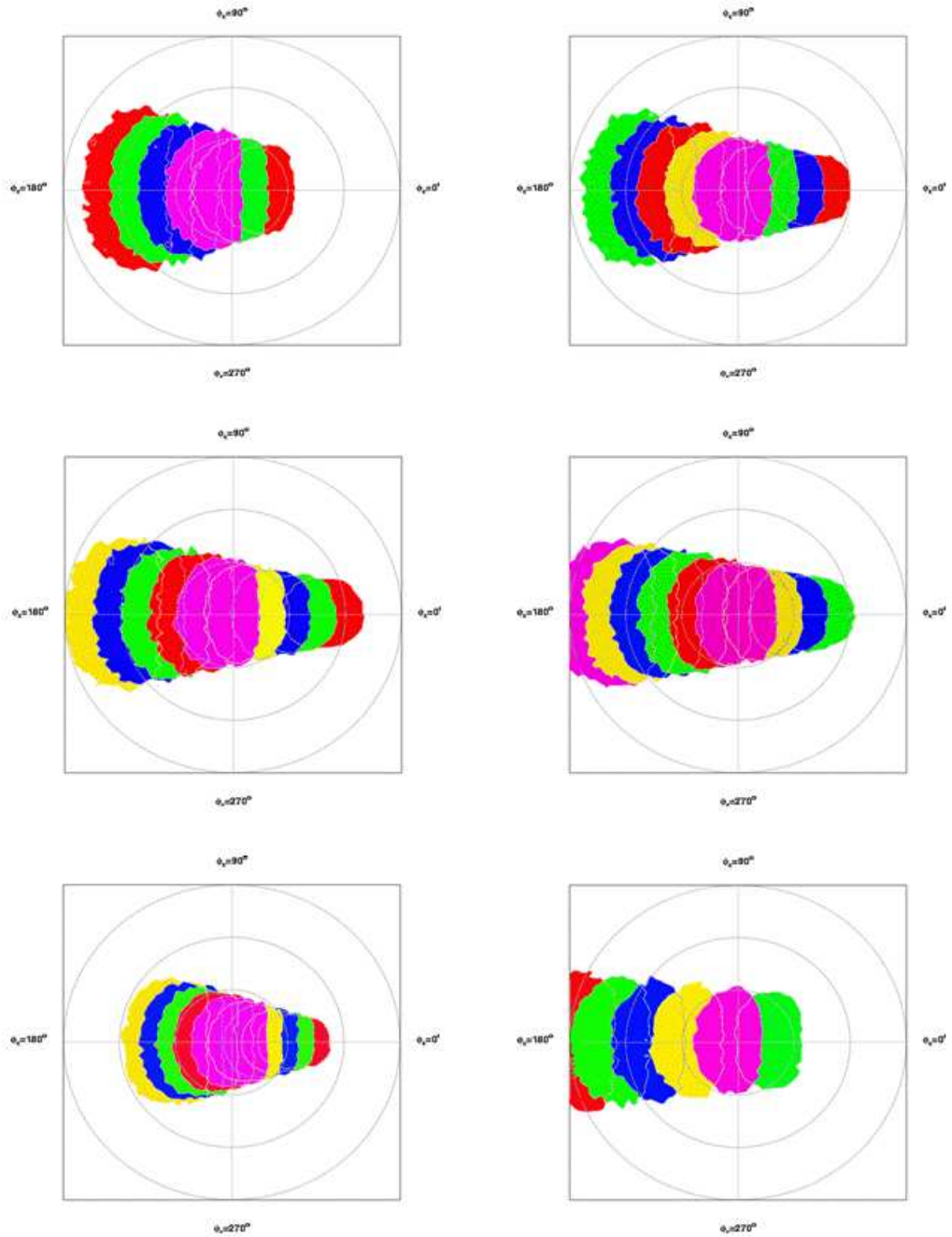

Figure 6: Coverage of proposed measurements in transverse momentum P_t and azimuthal angle ϕ (from top to bottom, left to right) for $(x,\ Q^2) = (0.20,\ 2.00\ \mathrm{GeV}^2)$, $(x,\ Q^2) = (0.30,\ 3.00\ \mathrm{GeV}^2)$, $(x,\ Q^2) = (0.40,\ 4.00\ \mathrm{GeV}^2)$, $(x,\ Q^2) = (0.50,\ 5.00\ \mathrm{GeV}^2)$, $(x,\ Q^2) = (0.30,\ 1.80\ \mathrm{GeV}^2)$, $(x,\ Q^2) = (0.30,\ 4.50\ \mathrm{GeV}^2)$ and $z = 0.40$. The different colors represent different θ_{pq} settings. The circles indicate $P_t = 0.2$, 0.4, and 0.6 GeV, respectively.

Table 1: Main kinematic settings for HMS.

E (GeV)	E' (GeV)	θ_e (deg)	W^2 (GeV^2)	θ_γ (deg)	q_γ (GeV)	Kinematics
11.0	5.67	10.27	8.88	10.57	5.513	I
11.0	5.67	12.59	7.88	12.75	5.603	II
11.0	5.67	14.55	6.88	14.49	5.692	III
11.0	5.67	16.28	5.88	15.96	5.779	IV
8.8	5.60	10.96	5.08	17.90	3.467	V
11.0	5.67	21.26	11.38	7.57	8.270	VI

4.2 Singles Rate Estimates

The DIS (e,e′) rates were calculated using the NMC fits for the structure functions F_1 and F_2. The singles e^- rates were calculated for a hydrogen target. The singles pion, kaon, and proton rates were estimated using parameterizations of SLAC data of Wiser *et al.* [32], also for a hydrogen target. For the deuterium target we will simply scale the beam intensity to keep the singles rates on the same level, which will minimize the systematic errors in the tracking efficiency.

We simply took a solid angle of 4 msr and a momentum acceptance of 30% for the singles rate estimates, which is a reasonable compromise between the HMS and SHMS acceptances. Beam currents were varied to limit the rates in the hadron spectrometer to approximate 700 kHz, to enable clean tracking and detection efficiency algorithms.

In all cases, the singles rates found were not too different from those given in proposal E12-06-104. We include the relevant information on the singles rates for hydrogen target as seen by the electron and hadron arm, and some relevant particle type ratios, in the extensive tables below that also include the coincidence rate information (see Tables 2, 3, 4, 5, 6 and 7).

We assume that for deuterium target the cross section will go up by a factor 2, and to keep rates on the same level as for hydrogen we will reduce beam current accordingly.

Note that for the E12-06-104 proposal we also considered the background due to pair production, but found this to be insignificant. The argument is repeated here: For electron-proton (deuteron) scattering there is a significant probability to produce neutral pions in the target, that can then, after decay, produce an electron-positron pair. Similarly, the Bethe-Heitler process can produce an electron-positron pair. Based on detailed studies in Halls B and C on such backgrounds, using a variety of nuclear targets, scattering angles, and spectrometer momenta, this background is considered insubstantial for the kinematics of interest. This is further substantiated with a 6 GeV test measurement in Hall C, where positrons were detected in SOS in coincidence with pions in HMS. Here, the background originating from π^0 production and its subsequent decay into two photons and then electron-positron pairs, was found to be negligible.

4.3 Coincidence Rate Estimates

We have added the possibility of semi-inclusive pion electroproduction to the general Hall C Monte Carlo package SIMC, following the high-energy expectation of factorization. We used the CTEQ5 next-to-leading-order (NLO) parton distribution functions to parameterize $q(x, Q^2)$ [33], and the fragmentation function parameterization for $D^+_{q\to\pi}(z, Q^2) + D^-_{q\to\pi}(z, Q^2)$, with D^+ (D^-) the favored (unfavored) fragmentation function, from Binnewies *et al.* [34]. The remaining unknowns are the ratio of D^-/D^+, the slope b of the P_t dependence, and the parameters A and B describing the ϕ dependence.

Both the D^-/D^+ ratio [27] and the b-value [35] were taken from HERMES analyses ($b \approx 4.66$). We assumed the parameters A and B to be zero for the count rate estimates. Our assumptions on b, A, and B do, however, not have a large an impact on the count rate estimates. The coincidence rate estimates, thus calculated, are given in Tables 2, 3, 4, 5, 6, and 7, in the form of the amount of time (in hours) required to accumulate 10K clean coincidence events.

Given the amount of overhead required in terms of target, spectrometer momentum and spectrometer polarity changes, we have used a one-hour limit as the minimum beam time request per kinematics setting. In almost all cases, less than one hour of beam time is required. In only a very few cases, typically at higher Q^2 and more forward SHMS angle, more than one hour of beam time would be required to accumulate 10K coincidence events (partly related to the increased hadron singles rates limiting the beam current). Nonetheless, we have kept the assumption of a one-hour beam time for these limited kinematics cases in the beam time request for this proposal.

An alternate approach, that in the end boils down to the same beam time estimate, is to limit the runs to ∼20 minutes in cases where the coincidence rates are large, and one still ends up with at least 10K "clean" coincidences (*i.e.*., corrected for random coincidences). In this case, we redistribute the beam time to now accumulate at least 10K statistics for *all* kinematics, even those that require more than one hour to obtain 10K. The total time required for each kinematics following this assumption is given at the bottom of Tables 2, 3, 4, 5, 6, and 7. A mix of these beam time assumption strategies would also allow us to fold in some possible beam time for dedicated runs to verify radiative correction assumptions, as described in Section 4.6.

4.4 Systematic Uncertainties

Since both the SHMS mechanical and optics design, and also the planned SHMS detector package, are essentially a clone of the HMS, we expect to achieve a similar high level of understanding of the SHMS acceptance function and detector properties. In this experiment, we plan to analyze the data in terms of a *comparison* of transverse momentum dependences of positive- and negative-charged pions, π^+ and π^-, and off hydrogen and deuterium targets.

Such comparisons are rather insensitive to external variations in rates due to *e.g.*, beam energy, scattering angle, and beam current, but are sensitive to differences in acceptance functions, detector efficiencies, and tracking efficiencies. The extended target acceptance of SHMS is designed to be nearly flat over an impressive target length, ≈ 20 cm as viewed under an angle of 90 degrees. In this experiment, we plan to use 10 cm extended targets only, with a maximum SHMS (HMS) angle of 28 (22) degrees. This corresponds to SHMS (HMS) to a maximum effective target length of 4.7 (3.7) cm, both small numbers compared to the nominal target

Table 2: Kinematic settings and rates for π^- (π^+) production on hydrogen for the (x, Q^2) = (0.20, 2.00 GeV^2) measurements, (main kinematics I). The coincidence time T_{coin} reflects the time needed (in hours) to accumulate 10K clean coincidence events. The accidental/real ratio within 2 nsec window is given in the A/R column, and is in general less than unity.

E (GeV)	E' (GeV)	θ_e (deg)	z	N_e (kHz)	π/e	I (μA)	θ_π (deg)	N_π (kHz)	T_{coin} (hour)	A/R
11.0	5.67	10.3	0.30	9 (7)	0.7	12 (10)	8.0	668 (889)	0.26 (0.38)	0.68 (0.96)
				13 (8)		19 (11)	10.5	667 (634)	0.16 (0.28)	0.65 (0.65)
				20 (12)		29 (17)	13.0	665 (627)	0.11 (0.19)	0.67 (0.67)
				32 (19)		46 (27)	15.5	663 (619)	0.08 (0.14)	0.75 (0.75)
				53 (31)		75 (43)	18.0	662 (612)	0.05 (0.08)	0.73 (0.73)
				53 (41)		75 (57)	20.5	401 (483)	0.05 (0.16)	0.73 (1.00)
				53 (53)		75 (75)	23.0	237 (372)	0.05 (0.16)	0.73 (1.00)
			0.40	11 (7)		15 (10)	8.0	659 (687)	0.12 (0.19)	0.45 (0.50)
				20 (12)		27 (16)	10.5	657 (611)	0.06 (0.11)	0.42 (0.42)
				35 (21)		50 (29)	13.0	654 (601)	0.04 (0.06)	0.44 (0.45)
				53 (40)		75 (56)	15.5	523 (591)	0.04 (0.04)	0.44 (0.53)
				53 (53)		75 (75)	18.0	268 (403)	0.04 (0.04)	0.44 (0.53)
				53 (53)		75 (75)	20.5	133 (198)	0.04 (0.04)	0.44 (0.53)
				53 (53)		75 (75)	23.0	65 (95)	0.04 (0.04)	0.44 (0.53)
			0.50	15 (9)		21 (13)	8.0	647 (600)	0.07 (0.12)	0.37 (0.37)
				31 (19)		44 (26)	10.5	644 (587)	0.03 (0.05)	0.33 (0.34)
				53 (41)		75 (57)	13.0	511 (575)	0.03 (0.03)	0.33 (0.37)
				53 (53)		75 (75)	15.5	225 (329)	0.03 (0.03)	0.33 (0.37)
				53 (53)		75 (75)	18.0	96 (137)	0.03 (0.03)	0.33 (0.37)
				53 (53)		75 (75)	20.5	39 (55)	0.03 (0.03)	0.33 (0.37)
				53 (53)		75 (75)	23.0	15 (21)	0.03 (0.03)	0.33 (0.37)

* *Total time (3 targets, 2 polarities with t_{min}=20 min at high rate) $\rightarrow T \simeq$ 3.5 days. Required time to change momenum (6), angles (42) and targets (126) $\rightarrow T \simeq$ 1.0 day. Subtotal time: $\rightarrow T \simeq$ 4.5 days.*

Table 3: Kinematic settings and rates for the ($x,\ Q^2$) = (0.30, 3.00 GeV^2) measurements (main kinematics II).

E (GeV)	E' (GeV)	θ_e (deg)	z	N_e (kHz)	π/e	I (μA)	θ_π (deg)	N_π (kHz)	T_{coin} (hour)	A/R
11.0	5.67	12.6	0.30	2 (3)	0.4	10 (10)	5.5	771 (1302)	1.01 (1.35)	0.82 (1.44)
				2 (3)		13 (10)	8.0	668 (890)	0.76 (1.10)	0.72 (1.00)
				5 (3)		19 (11)	10.5	666 (633)	0.43 (0.74)	0.64 (0.64)
				7 (4)		30 (17)	13.0	665 (626)	0.27 (0.46)	0.63 (0.63)
				12 (7)		47 (27)	15.5	663 (618)	0.18 (0.31)	0.66 (0.66)
				20 (11)		75 (45)	18.0	640 (611)	0.18 (0.21)	0.66 (0.73)
				20 (20)		75 (75)	20.5	382 (602)	0.18 (0.21)	0.66 (0.73)
				20 (20)		75 (75)	23.0	224 (350)	0.18 (0.21)	0.66 (0.73)
				20 (20)		75 (75)	25.5	129 (200)	0.18 (0.21)	0.66 (0.73)
			0.40	2 (3)		10 (10)	5.5	713 (1161)	0.69 (0.87)	0.60 (1.03)
				4 (3)		16 (10)	8.0	658 (673)	0.38 (0.61)	0.51 (0.55)
				7 (4)		28 (17)	10.5	656 (610)	0.17 (0.29)	0.43 (0.43)
				13 (8)		51 (31)	13.0	653 (599)	0.09 (0.15)	0.41 (0.41)
				19 (14)		75 (59)	15.5	496 (590)	0.09 (0.08)	0.41 (0.44)
				19 (19)		75 (75)	18.0	251 (376)	0.09 (0.08)	0.41 (0.44)
				19 (19)		75 (75)	20.5	124 (183)	0.09 (0.08)	0.41 (0.44)
				19 (19)		75 (75)	23.0	59 (87)	0.09 (0.08)	0.41 (0.44)
				19 (19)		75 (75)	25.5	27 (40)	0.09 (0.08)	0.41 (0.44)
			0.50	5 (3)		11 (10)	5.5	644 (943)	0.61 (0.80)	0.54 (0.85)
				5 (3)		22 (13)	8.0	646 (598)	0.23 (0.39)	0.44 (0.44)
				11 (7)		45 (27)	10.5	643 (585)	0.08 (0.13)	0.35 (0.35)
				20 (14)		75 (60)	13.0	482 (573)	0.08 (0.06)	0.35 (0.33)
				20 (20)		75 (75)	15.5	210 (305)	0.08 (0.06)	0.35 (0.33)
				20 (20)		75 (75)	18.0	88 (125)	0.08 (0.06)	0.35 (0.33)
				20 (20)		75 (75)	20.5	35 (50)	0.08 (0.06)	0.35 (0.33)
				20 (20)		75 (75)	23.0	13 (19)	0.08 (0.06)	0.35 (0.33)
				20 (20)		75 (75)	25.5	5 (7)	0.08 (0.06)	0.35 (0.33)

* *Total time (3 targets, 2 polarities with t_{min}=20 min at high rate) $\rightarrow T \simeq$ 4.5 days. Required time to change momenum (6), angles (54) and targets (162) $\rightarrow T \simeq$ 1.5 day. Subtotal time: $\rightarrow T \simeq$ 6.0 days.*

Table 4: Kinematic settings and rates for the ($x,\ Q^2$) = (0.40, 4.00 GeV^2) measurements (main kinematics III).

E (GeV)	E' (GeV)	θ_e (deg)	z	N_e (kHz)	π/e	I (μA)	θ_π (deg)	N_π (kHz)	T_{coin} (hour)	A/R
11.0	5.67	14.5	0.30	1 (1)	0.2	10 (10)	5.5	771 (1299)	3.55 (4.91)	1.06 (1.85)
				1 (1)		13 (10)	8.0	667 (881)	1.94 (2.84)	0.75 (1.03)
				2 (2)		19 (11)	10.5	666 (632)	1.06 (1.83)	0.66 (0.66)
				3 (3)		30 (18)	13.0	664 (624)	0.64 (1.11)	0.64 (0.64)
				6 (4)		49 (28)	15.5	662 (617)	0.38 (0.66)	0.62 (0.62)
				9 (7)		75 (47)	18.0	614 (609)	0.38 (0.42)	0.62 (0.64)
				9 (9)		75 (75)	20.5	363 (570)	0.38 (0.41)	0.62 (0.64)
				9 (9)		75 (75)	23.0	211 (328)	0.38 (0.41)	0.62 (0.64)
				9 (9)		75 (75)	25.5	120 (186)	0.38 (0.41)	0.62 (0.64)
			0.40	2 (1)		10 (10)	5.5	707 (1149)	2.63 (3.48)	0.82 (1.41)
				2 (2)		16 (10)	8.0	658 (659)	1.03 (1.68)	0.56 (0.60)
				3 (3)		29 (17)	10.5	655 (608)	0.43 (0.72)	0.45 (0.45)
				6 (5)		54 (32)	13.0	652 (598)	0.21 (0.35)	0.42 (0.42)
				9 (7)		75 (62)	15.5	471 (588)	0.21 (0.17)	0.42 (0.41)
				9 (9)		75 (75)	18.0	236 (352)	0.21 (0.17)	0.42 (0.41)
				9 (9)		75 (75)	20.5	115 (169)	0.21 (0.17)	0.42 (0.41)
				9 (9)		75 (75)	23.0	54 (79)	0.21 (0.17)	0.42 (0.41)
				9 (9)		75 (75)	25.5	25 (36)	0.21 (0.17)	0.42 (0.41)
			0.50	1 (1)		11 (10)	5.5	643 (925)	2.72 (3.74)	0.84 (1.30)
				3 (2)		22 (13)	8.0	645 (596)	0.70 (1.18)	0.53 (0.54)
				5 (5)		47 (28)	10.5	642 (583)	0.21 (0.35)	0.38 (0.38)
				9 (7)		75 (64)	13.0	455 (570)	0.21 (0.13)	0.38 (0.34)
				9 (9)		75 (75)	15.5	195 (283)	0.21 (0.13)	0.38 (0.34)
				9 (9)		75 (75)	18.0	80 (114)	0.21 (0.13)	0.38 (0.34)
				9 (9)		75 (75)	20.5	32 (45)	0.21 (0.13)	0.38 (0.34)
				9 (9)		75 (75)	23.0	12 (17)	0.21 (0.13)	0.38 (0.34)
				9 (9)		75 (75)	25.0	4 (6)	0.21 (0.13)	0.38 (0.34)

* *Total time (3 targets, 2 polarities with t_{min}=20 min at high rate) $\rightarrow T \simeq$ 4.0 days. Required time to change momenum (6), angles (54) and targets (162) $\rightarrow T \simeq$ 1.5 day. Subtotal time: $\rightarrow T \simeq$ 5.5 days.*

Table 5: Kinematic settings and rates for the $(x,\ Q^2) = (0.50,\ 5.00\ \mathrm{GeV}^2)$ measurements (main kinematics IV).

E (GeV)	E' (GeV)	θ_e (deg)	z	N_e (kHz)	π/e	I (μA)	θ_π (deg)	N_π (kHz)	T_{coin} (hour)	A/R
11.0	5.67	16.3	0.30	1 (1)	0.1	13 (10)	8.0	667 (872)	4.51 (6.62)	0.74 (1.01)
				1 (1)		20 (11)	10.5	666 (631)	2.65 (4.58)	0.69 (0.69)
				2 (1)		31 (18)	13.0	664 (623)	1.45 (2.51)	0.62 (0.62)
				3 (2)		50 (29)	15.5	662 (615)	0.83 (1.43)	0.59 (0.59)
				4 (3)		75 (49)	18.0	590 (608)	0.83 (0.89)	0.59 (0.61)
				4 (4)		75 (75)	20.5	346 (541)	0.83 (0.89)	0.59 (0.61)
				4 (4)		75 (75)	23.0	199 (308)	0.83 (0.89)	0.59 (0.61)
				4 (4)		75 (75)	25.5	112 (173)	0.83 (0.89)	0.59 (0.61)
				4 (4)		75 (75)	28.0	62 (95)	0.83 (0.89)	0.59 (0.61)
			0.40	1 (1)		16 (10)	8.0	657 (645)	2.65 (4.38)	0.60 (0.63)
				2 (1)		30 (18)	10.5	655 (607)	1.14 (1.92)	0.50 (0.50)
				3 (2)		56 (33)	13.0	652 (596)	0.48 (0.80)	0.42 (0.42)
				4 (3)		75 (65)	15.5	448 (586)	0.48 (0.37)	0.42 (0.39)
				4 (4)		75 (75)	18.0	221 (330)	0.48 (0.37)	0.42 (0.39)
				4 (4)		75 (75)	20.5	106 (156)	0.48 (0.37)	0.42 (0.39)
				4 (4)		75 (75)	23.0	49 (72)	0.48 (0.37)	0.42 (0.39)
				4 (4)		75 (75)	25.5	22 (32)	0.48 (0.37)	0.42 (0.39)
				4 (4)		75 (75)	28.0	10 (14)	0.48 (0.37)	0.42 (0.39)
			0.50	1 (1)		23 (14)	8.0	644 (594)	2.00 (3.36)	0.62 (0.63)
				3 (2)		49 (30)	10.5	640 (581)	0.61 (1.02)	0.46 (0.46)
				4 (3)		75 (67)	13.0	430 (568)	0.61 (0.32)	0.46 (0.35)
				4 (4)		75 (75)	15.5	182 (263)	0.61 (0.32)	0.46 (0.35)
				4 (4)		75 (75)	18.0	74 (105)	0.61 (0.32)	0.46 (0.35)
				4 (4)		75 (75)	20.5	29 (40)	0.61 (0.32)	0.46 (0.35)
				4 (4)		75 (75)	23.0	11 (15)	0.61 (0.32)	0.46 (0.35)
				4 (4)		75 (75)	25.5	4 (5)	0.61 (0.32)	0.46 (0.35)
				4 (4)		75 (75)	28.0	1 (2)	0.61 (0.32)	0.46 (0.35)

* *Total time (3 targets, 2 polarities with t_{min}=20 min at high rate) $\rightarrow T \simeq$ 4.0 days. Required time to change momenum (6), angles (54) and targets (162) $\rightarrow T \simeq$ 1.5 day. Subtotal time: $\rightarrow T \simeq$ 5.5 days.*

Table 6: Kinematic settings and rates for the (x, Q^2) = (0.30, 1.80 GeV^2) measurements (main kinematics V).

E (GeV)	E' (GeV)	θ_e (deg)	z	N_e (kHz)	π/e	I (μA)	θ_π (deg)	N_π (kHz)	T_{coin} (hour)	A/R
8.8	5.60	11.0	0.30	9 (9)	0.1	10 (10)	8.0	501 (928)	1.47 (1.71)	1.66 (3.15)
				12 (9)		11 (10)	10.5	431 (735)	0.84 (0.79)	1.00 (1.75)
				13 (9)		13 (10)	13.0	387 (567)	0.90 (0.93)	1.00 (1.51)
				18 (9)		17 (10)	15.5	409 (429)	0.58 (0.96)	1.00 (1.09)
				26 (14)		24 (13)	18.0	421 (404)	0.39 (0.74)	1.00 (1.00)
				34 (17)		31 (17)	20.5	409 (391)	0.32 (0.60)	1.00 (1.00)
				44 (23)		40 (21)	23.0	379 (360)	0.29 (0.55)	1.00 (1.00)
				82 (35)		75 (32)	25.5	514 (397)	0.29 (0.29)	1.00 (1.00)
				82 (33)		75 (28)	28.0	368 (244)	0.29 (0.88)	1.00 (1.00)
				82 (82)		75 (75)	30.5	261 (464)	0.29 (0.88)	1.00 (1.00)
			0.40	9 (9)		10 (10)	8.0	499 (880)	0.93 (1.01)	1.25 (2.28)
				18 (9)		17 (10)	10.5	606 (627)	0.27 (0.44)	1.00 (1.08)
				24 (13)		23 (13)	13.0	573 (546)	0.22 (0.40)	1.00 (1.00)
				39 (22)		36 (20)	15.5	622 (588)	0.12 (0.21)	1.00 (1.00)
				60 (33)		56 (31)	18.0	642 (603)	0.07 (0.13)	1.00 (1.00)
				82 (49)		75 (44)	20.5	563 (563)	0.07 (0.10)	1.00 (1.00)
				82 (82)		75 (75)	23.0	365 (612)	0.07 (0.10)	1.00 (1.00)
				82 (82)		75 (75)	25.5	233 (389)	0.07 (0.10)	1.00 (1.00)
				82 (82)		75 (75)	28.0	147 (244)	0.07 (0.10)	1.00 (1.00)
				82 (82)		75 (75)	30.5	91 (151)	0.07 (0.10)	1.00 (1.00)
			0.50	9 (9)		10 (10)	8.0	448 (764)	0.91 (0.87)	1.08 (1.93)
				24 (14)		23 (13)	10.5	663 (630)	0.15 (0.27)	0.96 (0.97)
				39 (22)		36 (21)	13.0	662 (622)	0.10 (0.17)	0.97 (0.97)
				63 (36)		59 (34)	15.5	661 (614)	0.05 (0.09)	0.87 (0.87)
				82 (60)		75 (56)	18.0	499 (607)	0.05 (0.05)	0.87 (0.84)
				82 (82)		75 (75)	20.5	292 (470)	0.05 (0.05)	0.87 (0.84)
				82 (82)		75 (75)	23.0	167 (267)	0.05 (0.05)	0.87 (0.84)
				82 (82)		75 (75)	25.5	94 (149)	0.05 (0.05)	0.87 (0.84)
				82 (82)		75 (75)	28.0	52 (82)	0.05 (0.05)	0.87 (0.84)
				82 (82)		75 (75)	30.5	28 (44)	0.05 (0.05)	0.87 (0.84)

* *Total time (3 targets, 2 polarities with t_{min}=20 min at high rate) $\rightarrow T \simeq$ 5.5 days. Required time to change momenum (6), angles (60) and targets (180) $\rightarrow T \simeq$ 1.5 day. Subtotal time: $\rightarrow T \simeq$ 7.0 days.*

Table 7: Kinematic settings and rates for the ($x,\ Q^2$) = (0.30, 4.50 GeV^2) measurements (main kinematics VI).

E (GeV)	E' (GeV)	θ_e (deg)	z	N_e (kHz)	π/e	I (μA)	θ_π (deg)	N_π (kHz)	T_{coin} (hour)	A/R
11.0	3.0	21.3	0.30	1 (1)	12.6	10 (10)	5.5	666 (1072)	4.89 (5.71)	0.31 (0.53)
				1 (1)		17 (11)	8.0	654 (611)	2.55 (4.30)	0.29 (0.29)
				1 (1)		34 (20)	10.5	651 (599)	1.49 (2.50)	0.32 (0.32)
				1 (1)		68 (41)	13.0	648 (588)	0.97 (1.62)	0.39 (0.39)
				1 (1)		75 (75)	15.5	347 (517)	0.97 (1.58)	0.39 (0.39)
				1 (1)		75 (75)	18.0	162 (238)	0.97 (1.58)	0.39 (0.39)
				1 (1)		75 (75)	20.5	73 (106)	0.97 (1.58)	0.39 (0.39)
			0.40	1 (1)		13 (10)	5.5	628 (739)	2.29 (3.18)	0.20 (0.26)
				1 (1)		31 (18)	8.0	630 (576)	0.91 (1.52)	0.19 (0.19)
				1 (1)		74 (45)	10.5	626 (560)	0.44 (0.73)	0.22 (0.22)
				1 (1)		75 (75)	13.0	244 (351)	0.44 (0.73)	0.22 (0.22)
				1 (1)		75 (75)	15.5	90 (126)	0.44 (0.73)	0.22 (0.22)
				1 (1)		75 (75)	18.0	31 (43)	0.44 (0.73)	0.22 (0.22)
				1 (1)		75 (75)	20.5	10 (14)	0.44 (0.73)	0.22 (0.22)
			0.50	1 (1)		20 (12)	5.5	583 (545)	1.27 (2.10)	0.16 (0.17)
				1 (1)		57 (35)	8.0	585 (528)	0.38 (0.63)	0.15 (0.15)
				1 (1)		75 (75)	10.5	242 (347)	0.38 (0.63)	0.15 (0.15)
				1 (1)		75 (75)	13.0	72 (99)	0.38 (0.63)	0.15 (0.15)
				1 (1)		75 (75)	15.5	20 (27)	0.38 (0.63)	0.15 (0.15)
				1 (1)		75 (75)	18.0	5 (7)	0.38 (0.63)	0.15 (0.15)
				1 (1)		75 (75)	20.5	1 (1)	0.38 (0.63)	0.15 (0.15)

* *Total time (3 targets, 2 polarities with t_{min}=20 min at high rate) $\rightarrow T \simeq$ 3.0 days. Required time to change momenum (6), angles (42) and targets (126) $\rightarrow T \simeq$ 1.0 day. Subtotal time: $\rightarrow T \simeq$ 4.0 days.*

length acceptances of the magnetic spectrometers. Thus, we expect the systematic uncertainty in acceptance functions for such target ratios to be small.

The advantage of using highly-focusing magnetic spectrometers with a well-defined optics is that they are well reproducible, even when changing polarities. The spectrometer momenta used in this experiment are nearly constant for the electron detector, HMS, ≈ 5.67 GeV, and range from roughly 1.5 to 3 GeV for the hadron detector, SHMS. For the HMS, reproducibility of the magneto-optics properties are well proven at this central momentum (and, no polarity changes are foreseen either way). For SHMS, this momentum range is far from the region where one would need to worry about saturation or reproducibility effects. We do note that the present plan is to map the Horizontal Bend dipole magnet, to measure multipole components and central magnetic axis for the three SHMS quadrupole magnets, the former as function of magnet current, and to equip the three quadrupole magnets with Hall probes and the large dipole magnet with an NMR probe, such that reproducibility can be readily checked.

As can be verified from the previous tables of rate estimates (see Tables 2, 3, 4, 5, 6, and 7), we have limited the hadron rates to a maximum of 700 kHz (with the pion rates in all cases to be by far the dominant contribution). Since rates on hydrogen and deuterium targets will differ, and (γ, π^+) and (γ, π^-) will differ, this will introduce a variation in beam currents for the various ratios. However, the beam current variation is relatively modest (about a factor of 30% from π^+ to π^-, and a factor of 2 from hydrogen to deuterium), and in all cases SIDIS pion yields will be normalized to inclusive electron yields.

This leaves uncertainties in detector and tracking efficiencies. The electron rates are modest (less than 100 kHz), and the pion to electron ratio for the electron detection arm reasonably low (13 or lower), such that the HMS performance for tracking efficiency and electron identification and efficiency will be well understood, with a negligible uncertainty. The main systematic uncertainties in the measured ratios will thus be due to the hadron tracking efficiency and the hadron detection efficiency.

To minimize the systematic uncertainties, we varied as mentioned above the beam current to get roughly constant hadron rates for all cases (hydrogen, deuterium, π^+, π^-), and limited the *total* SHMS rate to 700 kHz maximum. For HMS, the tracking efficiency was found to be rate dependent, which was up to about 500 kHz well understood in terms of Poisson statistics. This rate dependence will be reduced in SHMS due to the use of multi-hit TDCs, and the use of a wire chamber plane configuration that gives three independent x- and y-measurements. For the HMS chambers, four planes were roughly x-measurements, and only two planes gave y-measurements, which complicated the tracking in high rate conditions when two close-by tracks were in principle possible. For SHMS, we expect to get good systematic understanding of the tracking efficiencies up to about 1 MHz hadron rates (albeit with a lot of work!). However, since this experiment is mostly kinematic configuration change limited, we have used an upper and more comfortable cutoff of 700 kHz total rate here.

Given the redundancy in detector package in the SHMS, and the relatively low requirements for particle identification, we expect to understand the SHMS detector efficiencies to be at least as well as the HMS ones. Some pions will originate from kaons that decay before reaching the detectors, but this can be corrected for by using the measured kaon yields and the Monte Carlo simulation of the spectrometers, with a resulting uncertainty in yield ratios of about 0.1%, on average. In summary, we anticipate uncertainties for these *ratios* as given in Table 8. We note that Hall C has established point-to-point uncertainties for inclusive measurements in the

Table 8: Anticipated systematic uncertainties (in ratios of transverse momentum dependences). Note that this table assumes the combined use of the CLAS12 experiments to fully constrain the (P_t, ϕ) dependency.

Project Source	HMS	SHMS
Spectrometer Acceptance	0.1%	0.4%
Tracking Efficiency	0.1%	0.4%
Detection Efficiency	0.1%	0.4%
Pion Absorption Correction		0.1%
Pion Decay Correction		0.1%
Radiative Corrections		0.5%
Added in Quadrature		0.9%

range of 1.1-1.5%, and anticipates to obtain point-to-point uncertainties for far more challenging pion form factor measurements [36] and measurements of the ratio $R = \sigma_L/\sigma_T$ in SIDIS [31] of 1.6-1.8%. The quoted uncertainties in Table 8 are largely based upon projections of those experiments.

4.5 Diffractive vector meson contributions

Some of the events we will observe originate from the decay of diffractive vector meson production. The underlying physics of these processes, in which a virtual photon fluctuates into a vector meson, which interacts with the nucleon through multiple gluon exchange (i.e. Pomeron exchange), is distinctively different that the interaction of a virtual photon with a single current quark. As in our previous experiment [10], we plan to subtract the contributions of diffractive vector meson decay on a bin by bin basis, although we will also present the results without subtraction, in the case that improved knowledge of the diffractive ρ, ω, and higher mass vector resonances becomes available in the future.

In any case, we will make a fit to world data that is available at the time of the analysis of the results of this experiment, and use the SIMC Monte Carlo generator to evaluate the diffractive vector meson contribution to the counts in each kinematic bin. Based on HERMES simulations at somewhat similar kinematics as the present proposal [37], we expect the fraction of events from this "background" to range from a few percent at low z to about 15% at $z = 0.6$. The systematic error on our final results may range from 0.5% to 2%. We expect the error to be smaller on the ratios of cross sections, since equal rates of π^+ and π^- are expected for a given target. We did not include this uncertainty as contribution in Table 8, as these diffractive contributions have physics interest of themselves, and we will give any final results both with and without this contribution.

4.6 Radiative Corrections

We plan to make specific measurements to reduce the error in the ratios of cross sections from radiative corrections to 0.5%. As is well known, essentially all of the events that "radiate in" to

a given bin come from either: (i) electrons with a lower actual energy that the nominal beam energy, because they have radiated a photon along the incident beam direction; or (ii) scattered electrons with higher energy than the one measured in the spectrometer, because a photon was radiated along the scattered electron direction. In both cases, the value of ν at the vertex is lower than the nominal one, hence z (M_x) is larger (smaller) than the nominal one. While the probability of radiating a hard photon of a given energy is itself well known from QED [38], what is needed for accurate corrections is a good knowledge of the cross sections at lower E and higher E' than the nominal ones, for a given electron scattering angle and a given hadron momentum and angle. We plan to supplement cross section measurements that will be obtained in CLAS12 [39] and in E12-06-104 [31] with possible additional measurements. Even though the CLAS12 apparatus is foreseen to accumulate cross section measurements over a wide range of beam energies, particle momenta and angles, there are several reasons to augment those measurements with dedicated HMS-SHMS measurements. Amongst others: a) a desire to use the same high resolution spectrometers as for the main measurements; b) a good separation of pions, kaons and protons; c) use of the same target for all measurements (so that external radiative strength is constant); d) a common normalization error for all measurements. We propose to repeat a subset of the measurements at all nominally 11 GeV kinematics with 8.8 and 6.6 GeV beam energies. A specific beam time request for 6.6 GeV beam energy running is not included, as the approved E12-06-104 experiment already has dedicated running at this beam energy. The experimental run plans will be optimized in combination, might this proposal be approved.

We will also optimize which z and θ_{pq} setting we study to minimize the final error on radiative corrections. Lastly, for the 11 GeV kinematics, we will measure the rates with the electron momentum increased by 25%, and possibly 50%, for a sample of about one quarter of the settings. For cases where the HMS spectrometer can't go to such high momentum, we will reverse the roles of the HMS and SHMS spectrometers for these studies, and will only do angles where the hadron angles is greater than 10.5 degrees. Rates for such dedicated radiative correction measurements are large, and can easily be done in 15 minutes, even including overhead time to change angles. Once we determine an optimized set of points to run, we will reduce the running time for the production kinematics. (*i.e.*, if the factor is 0.7 to 0.8, which is a worst-case estimate, one hour runs will be reduced to about 45 to 50 minutes, or 20-minute runs to about 15 minutes) to keep the total beam request constant. The precision "spot" measurements of this study will be combined with all available world data to build the best possible model of cross sections a the kinematics that can "radiate in" to our production settings. Similar modeling efforts have been done for inclusive electron scattering measurements of hydrogen and deuterium targets by this group [40, 41].

5 Related Measurements

The main emphasis of this proposal is on using an unpolarized electron beam to map the transverse momentum dependence of charged pion $\pi^{\pm}$ electroproduction off hydrogen and deuterium targets. There are two additional measurements that are directly enabled by this proposal. A dedicated kaon identification detector to the SHMS base detector package, already inherent in multiple 12-GeV experiments ([31, 36, 42, 43], will now definitely augment the SHMS.

Construction for this dedicated kaon identification system has been recently approved as a Major Research Instrumentation grant of the National Science Foundation to a consortium of the Catholic University of America (lead), University of South Carolina, Mississippi State University, and Florida International University, with both the Yerevan Physics Institute and Jefferson Lab as collaborating institutions. The second additional measurement utilizes the highly-polarized CEBAF electron beam to determine pion (and kaon) single-spin asymmetries.

These two additional measurements, and their requirements, are presented in somewhat more detail in this Section.

5.1 Kaon Identification and Kaon Electroproduction

Kaon identification at kaon momenta up to 3 GeV/c will be performed using the combination of time-of-flight and a dedicated aerogel detector. The SHMS base detector package leaves some 60 cm of open space for dedicated particle identification detectors. Recently the construction of a pair of Aerogel detectors, essentially clones of the HMS Aerogel detector (that was constructed and commissioned by this group [44]) was approved by an NSF/MRI grant for construction. The dedicated kaon identification system will be constructed at a time scale such that it is ready at the start of the 12-GeV operations phase in Hall C.

We note that the addition of the aerogel detector system for the combined set of experiments formed by approved experiment E12-06-104 and this proposed experiment, would also allow comparable tests of the onset of low-energy factorization for semi-inclusive charged kaon electroproduction. This is in close analogy as we could do previously for charged-pion electroproduction with the 6-GeV E00-108 experiment [10]. A large data set of charged-kaon ($K^{\pm}$) electroproduction from both hydrogen and deuterium targets would be obtained spanning the low-energy residual-mass region up to the deep inelastic mass region, which could conclusively show the onset of the quark-hadron duality phenomenon for the case of kaons. The accumulated data would allow us to construct several ratios from these data to exhibit this phenomenon, and relate it to the high-energy factorization ansatz of electron-quark scattering and subsequent quark $\rightarrow$ kaon production mechanisms. Especially the "all-sea" case of K^- electroproduction may shed more light on the understanding of the quark-hadron duality and low-energy factorization phenomena.

We plan to extract ratios of favored to unfavored fragmentation functions in a certain framework, and test if this is independent of x and Q^2, in close analogy in the pion case studied by E00-108. Such a program will work hand-in-hand with the anticipated proton-deuteron ratio proposal to PAC-38 of CLAS12, which would in addition to studying the pions also allow charged kaons $K^{+/-}$ to be looked at with the CLAS12 detector. Similar to pions, the unpolarized ratios $d(e,e'h)X/p(e,e'h)X$ would be obtained for the charged kaons as functions of the hadron transverse momentum P_t and azimuthal angle ϕ. The CLAS12 proposal would highly benefit from the planned RICH detector [45], due to the particle identification capabilities needed for kaons.

Lastly, with measurements in hand to guide us where low-energy factorization is applicable for semi-inclusive kaon electroproduction, the addition of kaon identification might allow us to map the transverse momentum dependence for semi-inclusive charged-kaon electroproduction from proton and deuteron targets, in a subset of the proposed charged-pion measurements. Given that the proposed measurements correspond to an expected statistics of about 1K coincident kaons per kinematic setting, this is anticipated as sufficient for a first study of these transverse

momentum dependences.

5.2 Single-spin asymmetries

The asymmetry between cross sections with a longitudinally polarized beam either parallel or anti-parallel to an unpolarized target (refered to as the "beam single spin asymmetry (SSA), or A_{LU}), is an interesting quantity for the study of correlations in nucleon structure. The beam SSA has no leading twist contribution: the minimum order of twist is three. This makes it particularly sensitive to correlations such as those between quark and gluon momenta, and the correlations of quark spin with orbital motion. The beam SSA depends almost entirely on $\sin(\phi^*)$, with an amplitude relative to the base-line spin-averaged cross section of typically 0.02 to 0.06 at JLab or Hermes kinematics [37] for π^+, with values much closer to zero for π^-. The x, Q^2, z, and P_t dependence is significant (with the prominent features being an increase with increasing P_t and x, and a decrease with increasing Q^2), and can be qualitatively understood in di-quark models [46].

While the present proposal is not ideally suited to the measurement of beam SSAs, due to the lack of full ϕ^* coverage for $P_t > 0.3$ GeV, we can nonetheless make valuable contributions to the study of this process at low P_t, where we do have full ϕ^* coverage. Our measurements are complementary to those that will be carried out in CLAS, due to the better momentum and angular resolutions of the Hall C spectrometers. Based on previous experience, we estimate that we can go as low as $P_t = 0.05$ GeV before the resolution in ϕ^* becomes larger than $\pi/3$ (at which point the SSA starts to become reduced due to resolution effects). The typical lower cut in P_t for CLAS with 6 GeV has been about a factor of two larger (around 0.1 to 0.15 GeV). Our estimate is that we will be able to measure the beam SSA at $P_t = 0.05$, 0.10, 0.15, and 0.20 GeV with a statistic error of typically 0.003 to 0.008 for all of the kinematic settings except (x, Q^2) =(0.3, 4.5 GeV^2). We expect the systematic error to be smaller or at most comparable. Since we expect the π^+ asymmetries to be of order 0.02 to 0.04, our measurements will place significant constraints on models, and also allow for the first accurate determination of neutron SSA at low P_t.

We therefore request that the beam be longitudinally polarized for this experiment.

6 Projected Results

In order to get an idea of how well we can determine μ_d and μ_u from the proposed charged pion data, we binned the projected data into eight bins of P_t, fifteen bins in ϕ^*, and three bins in z for each of the six kinematic settings. We generated the pseudo-data using the function form assumed in the previous section, with ${\mu_d}^2 = {\mu_u}^2 = 0.2$ GeV^2. Each data point was randomly moved from it's ideal point using a Gaussian distribution about the expected statistic error for that point. We fit the data with the same seven parameters as for the previous Hall C experiment. With these assumptions, we found an error ellipse that is so small that it essentially looks like a *single point* on a plot of ${\mu_d}^2$ and ${\mu_u}^2$, when all six kinematics are included in the fit simultaneously.

We then added four more parameters, all reflecting different simplifications generally assumed in the analysis of SIDIS data. The first treats the power of $(1 - z)$ for the ratio of favored to

unfavored fragmentations as a free parameter, rather than this power being fixed at -2. The next two allow for the possibility that there are two different favored fragmentation functions (one for π^+ from u quarks, and a different one for π^- from d quarks), differing by an unknown power of $(1-z)$. This similarly allows for two unfavored fragmentation functions. A fourth parameter allows for a charge-symmetry violation between neutron and proton, along the lines of the recent MRST fit [47]. With all six kinematic settings averaged together, the error ellipse *remains small, with a diameter of less than 0.01 GeV*^{2}.

As a next step, we fitted each kinematic setting separately. This provides a good way to check that the data is consistent with the model, if the error ellipses overlap. We show the result for the eleven parameter fit described above in Fig. 7a. It can be seen that the error ellipse is smallest for the $x = 0.2$ setting (black), due to the high event rates, and largest for the low rate $x = 0.3$, $Q^2 = 4.5$ GeV^2 setting (green), but it is important to note that each setting on it's own makes a reasonable determination. Combining the settings together results in the very small error refered to above (an error ellipse with diameter of less than 0.01), due the constraints in the x and Q^2 variations in the fit form.

The very high statistical precision and broad coverage in most kinematic variables (except ϕ^* at larger P_t), allows for even more fit parameters. Thus, as a next step we added eight more parameters to this exercise to mimic a possible higher-twist contribution. Four of these reflect (one each for proton and deuteron for π^+ and π^-) a possible higher-twist correction of the form $P_t^2/Q^2\cos(\phi^*)$. Four more parameters reflect higher-twist terms of the form $(P_t^2/Q^2)\cos(2\phi^*)$. While the coefficients of these terms are relatively poorly determined, the errors on ${\mu_u}^2$ and ${\mu_d}^2$ only increased by about a factor of two, as shown in Fig. 7b.

As a last step, we investigated one of the larger uncertainties in the model we used: the strength of the Cahn term. To investigate this, we simulated the data without this term, and also assumed it was absent in the fit. The results are shown in Fig. 7c, and remain rather similar to those with the Cahn term included (Fig. 7b). If we again do a simultaneous fit to *all* six kinematic settings, we still obtain a small error ellipse, with an average diameter of 0.02 GeV^2.

There are many other parameters that could potentially be added to the model, such as those describing sea quark contributions, and additional terms in P_t. Ideally, the analysis should be done in NLO rather than LO QCD. All of this will be possible due to the significant range in x, Q^2, z, and P_t of this proposal. Nonetheless, the above studies already give strong indications that a robust determination of transverse quark momentum widths should be possible, even with more complex treatments.

Finally, we also illustrate the projected uncertainties for charged kaons as a function of P_t in Fig. 8. The projected data are shown for $x = 0.30$, $Q^2 = 3.0$ GeV^2, and $z = 0.4$ (at a beam energy of 11.0 GeV). It is clear that a high-quality set of charged-kaon data off proton and deuteron targets will be attained in this experiment, over a range of x, Q^2, and z compatible with the proposed charged-pion data.

6.1 Contribution to the base Equipment of Hall C

The Yerevan group with Hamlet Mkrtchyan as one of the spokespersons of this proposal has taken on responsibility of assembling and testing the calorimeter for the SHMS. The blocks and PMTs for this calorimeter are a contribution to the 12-GeV Upgrade project by Yerevan and NIKHEF. The Yerevan group has also worked on the research and design related to the choice

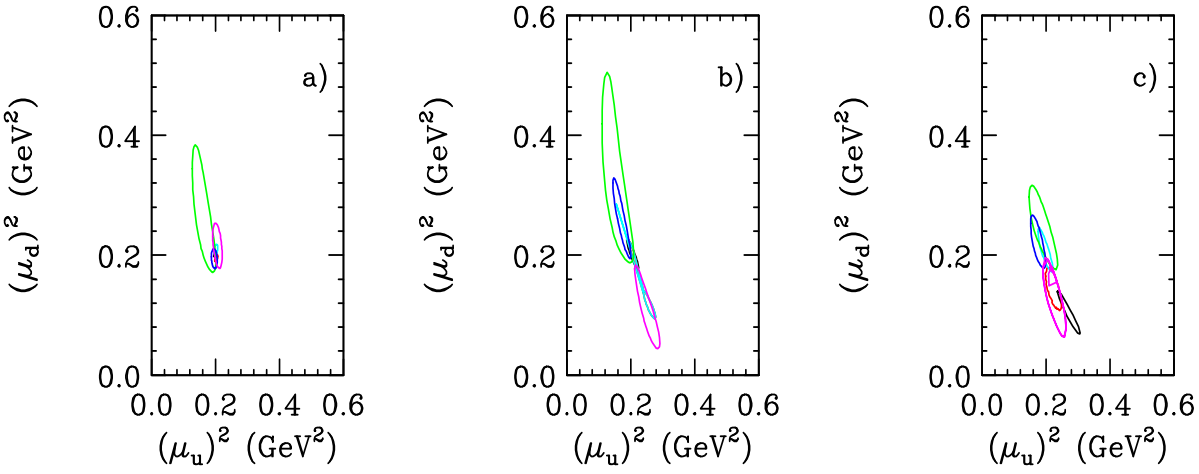

Figure 7: Error contours for $\mu_u{}^2$ versus $\mu_d{}^2$ for: a) Cahn term on, no higher twist terms; b) Cahn term on, with higher twist terms; c) Cahn term off, with higher twist terms. On each plot, kinematics I, II, III, IV, V, and VI are colored black, cyan, blue, magenta, red, and green, respectively. Fits taking all six kinematics simultaneously into account render an error ellipse of diameter 0.01 GeV^2 for panel a), and 0.02 GeV^2 for panels b) and c) (see text).

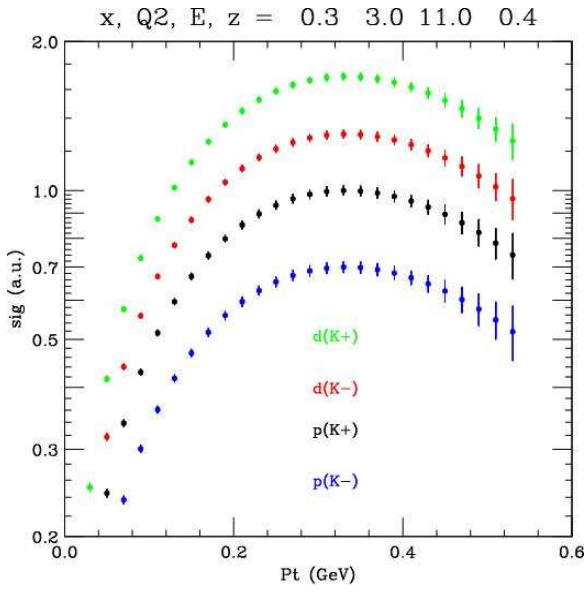

Figure 8: An example of the projected charged-kaon data for $x = 0.30$, $Q^2 = 3.0$ GeV^2, and $z = 0.4$.

of calorimeter blocks, and confirmation of the suitability of the contributed calorimeter blocks (previously used in the HERMES experiment), and the engineering and design. The preshower detector will consist of calorimeter blocks presently in the SOS spectrometer. The Yerevan group is committed to further construction and subsequent commissioning of the complete SHMS electromagnetic calorimeter.

Given their lead role in the design and construction of the HMS aerogel detector, the Yerevan group plans to collaborate to the extent possible with the consortium (Catholic University of America, University of South Carolina, Mississippi State University, and Florida International University) that recently was awarded an NSF/MRI grant for construction of an SHMS kaon identification system, consisting of a pair of aerogel detectors.

The Hampton group (M.E. Christy, R. Ent, C.E. Keppel, P. Monaghan et al.) are part of a consortium (with the College of William and Mary (lead), James Madison University and North Carolina A&T), that have obtained funding from the National Science Foundations's Major Research Instrumentation program to construct the SHMS tracking and trigger detectors (consisting of the wire chambers, scintillators, quartz detector, and their detector frame). Hampton's commitment in this consortium is to the (design and) construction and commissioning of the SHMS wire chambers.

Further collaborators of this proposal have taken lead roles for the construction of the SHMS scintillator systems (James Madison University), the SHMS quartz detection system (North Carolina A&T), and the two SHMS Cherenkov detectors (University of Regina and University of Virginia).

7 Summary and Beam Time Request

We request a total of 32 days of beam time to map the transverse momentum (P_t) dependence for semi-inclusive electroproduction of charged pions ($\pi^{\pm}$) and kaons ($K^{\pm}$) from both proton and deuteron targets over the range $0.2 < x < 0.5$, $2 < Q^2 < 5$ GeV^2, $0.3 < z < 0.5$, and $P_t < 0.5$ GeV, with the Hall C HMS-SHMS magnetic spectrometer coincidence pair. We request a polarized electron beam to add the possibility to determine single-spin asymmetries from these measurements.

The proposed measurements emphasize the low P_t region, of scale Λ, where one-particle inclusive deep inelastic scattering off polarized and unpolarized nucleons has been analyzed, using tree-level factorization, for low transverse momentum of the scattered hadron. To better constrain possible $P_t - \phi$ correlations in the region $0.2 < P_t < 0.5$ GeV, it is envisioned that this experiment is a companion of the experimental program with the large acceptance CLAS12 detector, with unpolarized hydrogen and deuterium targets, such as that approved for E12-06-112 [39]. This experiment will provide the very best measurements of the *ratios* of π^+ to π^- cross sections, both for hydrogen and deuterium targets, given the close symmetry between detection of positive- and negative-charged pions with a focusing magnetic spectrometer pair setup.

A summary of our beam time request is given in Table 9, and amounts to 32 days. The beam currents are chosen to limit the total singles rates in the hadron spectrometer to a maximum of 700 kHz, but this does not impact the requested beam time given that the coincidence rates are generally high (the beam current for deuterium running will be adjusted such that the singles rates are similar to those for hydrogen).

Table 9: Beam time request

E (GeV)	Target	Time (Hours)
8.8	LH2	54
	LD2	54
	Al	14
11.0	LH2	206
	LD2	206
	Al	52
	Checkout	0 (overlap with E12-06-104)
	Momentum Changes (36)	18
	Angle Changes (306)	20
	Target Changes (918)	150
	Pass Changes (1)	0 (overlap with E12-06-104)
	Beam Energy Measurements (2)	0 (overlap with E12-06-104)
	Total Request	774

We assume one-hour runs for hydrogen and deuterium targets each, for each setting of x, Q^2, z and θ_{pq}, which will give at least 10K clean coincidence events for each setting (possibly barring a few selected cases, where we will accumulate a few thousand coincidences). For electro-produced charged kaons, the rates will be close to a factor of ten reduced.

We further assume to run 25% of the time on the Al "dummy" target (15-minute runs), for subtraction of end-wall purposes. By choice of kinematics of overlap with experiment E12-06-104, we have saved several settings, and overhead for checkout, pass changes and beam energy measurements, corresponding to about 5 days of beam time. Time for further configuration changes has been outlined, and is assumed to amount to 30 minutes for each spectrometer momentum change, 5 minutes for each (small) spectrometer angle change, and 10 minutes for each target change. This is identical to the overhead assumptions in the approved E12-06-104 experiment.

References

[1] A. Bachetta, M. Diehl, K. Goeke, A. Metz, P.J. Mulder, and M. Schlegel, JHEP **0702**, 093 (2007).

[2] J. Ashman *et al.*, Phys. Lett. **B 206**, 364 (1988), Nucl. Phys. **B 328**, 1 (1989).

[3] P. L. Anthony *et al.*, Phys. Lett. **B 458**, 529 (1999); **B 463**, 339 (1999); **B 493**, 19 (2000).

[4] A. Airapetian *et al.*, Phys. Lett. **B 404**, 383 (1997); **B 444**, 531 (1998) Phys. Lett. **B 442**, 484 (1998).

[5] J. Adams *et al.*, Phys. Rev. Lett. **92**, 171801 (2004); S. S. Adler *et al.*, Phys. Rev. Lett. **91**, 241803 (2003).

[6] X. Ji *et al.*, Phys. Lett. **B 597**, 299 (2004).

[7] M. Anselmino, M. Boglione, U. D'Alesio, A. Kotzinian, F. Murgia and A. Prokudin, AIP Conf. Proc. **792**, 981 (2005) [arXiv:hep-ph/0507157]; M. Anselmino, M. Boglione, A. Prokudin and C. Turk, Eur. Phys. J. A **31**, 373 (2007) [arXiv:hep-ph/0606286]; M. Anselmino *et al.*, Phys. Rev. **D71** (2005) 074006; M. Anselmino, M. Boglione, A. Prokudin, and C. Turk, Eur. Phys. J. **A31** (2007) 373.

[8] H. Mkrtchyan *et al.*, Phys. Lett. **B665** (2008) 20.

[9] W. Melnitchouk, AIP Conf. Proc. **588**,(2001) 267; W. Melnitchouk, R. Ent and C.E. Keppel, Phys. Rep. 406 (2005) 127.

[10] T. Navasardyan *et al.*, Phys. Rev. Lett. **98** (2007) 022001. E00-108 experiment, spokespersons: R. Ent, H. Mkrtchyan, and G. Niculescu.

[11] J. T. Dakin *et al.*, Phys. Rev. Lett. **31**, 786 (1973).

[12] A.S. Raskin and T.W. Donnelly, Ann. Phys., **191**, 78 (1989).

[13] R. N. Cahn, Phys. Lett. **B 78**, 269 (1978); Phys. Rev. D **40** 3107 (1989).

[14] J. Levelt and P. J. Mulders, Phys. Rev. **D 49**, 96 (1994).

[15] E. L. Berger, T. Gottschalk, and D. W. Sivers Phys. Rev. D **23** (1981) 99.

[16] K. Oganessyan *et al.*, Eur. Phys. J. C5 (1998) 681.

[17] A. Metz, Phys. Lett. **B549** (2002) 139.

[18] A. Bacchetta *et al.* JHEP 0702 (2007), 93.

[19] D. Boer and P. J. Mulders, Phys. Rev. D **57** (1998) 5780; Nucl. Phys. **B564** (2000) 471; D. Boer and R. D. Tangerman, Nucl. Phys. **B 461** (1996) 197.

[20] Vincenzo Barone, Zhun Lu and Bo-Qiang Ma, hep-ph/0512145 (2005).

[21] L P. Gamberg, G. R. Goldstein, and M. Schlegel, Phys. Rev. D **77** (2008) 094016; hep-ph/0708.0324

[22] A. Afanasev *et al.*, Phys. Rev. D **66** 074004 (2002).

[23] N. Makins, Ph. D. Thesis, Massachusetts Institute of Technology (1994), unpublished; R. Ent *et al.*, Phys. Rev. C **64**, 054610 (2001).

[24] P. Schweitzer, T. Teckentrup, and A. Metz, Phys. Rev. D **81**, 094019 (2010).

[25] M. Osipenko *et al.*, Phys. Rev. D **80**, 032004 (2009).

[26] M. Glück, E. Reya, and A. Vogt, Eur. Phys. J. **C5** (1998) 461.

[27] P. Geiger, Ph.D. Dissertation, Ruprecht Karl Uniiversitat, Heidelberg, Germany, (1998), unpublished; Hermes Internal Note 98-005.

[28] R. Jakob, P.J. Mulders, and J. Rodrigues, Nucl. Phys. **A626**, 937 (1997).

[29] Bino Maiheu, Ph.D Thesis, Universiteit Gent, March 2006 (HERMES DOC 06-061).

[30] M. Lacombe *et al.*, Phys. Rev. C **21**, 861 (1980).

[31] *Measurement of the Ratio $R = \sigma_L/\sigma_T$ in Semi-Inclusive Deep Inelastic Scattering*, PAC-30 E12-06-104 proposal, spokespersons: R. Ent and H. Mkrtchyan.

[32] D.E. Wiser, Ph.D thesis, U. Wisconsin, 1977 (unpublished).

[33] H.L. Lai *et al.*, Eur. Phys. J. **C12** (2000) 375.

[34] J. Binnewies, B. A. Kniehl, and G. Kramer, Phys. Rev. D **52** (1995) 4947.

[35] B. Hommez, Ph. D. Dissertation, Gent University (2003), unpublished.

[36] *Measurement of the Charged Pion Form Factor to High Q^2*, PAC-30 E12-06-101 proposal, spokespersons: G.M. Huber and D. Gaskell.

[37] HERMES Collaboration (A. Airapetian *et al.*), Phys. Lett. **B 648** (2007) 164.

[38] L. W. Mo, Y. S. Tsai, *"Radiative Corrections to Elastic and Inelastic ep and μp Scattering"*, Rev. Mod. Phys. **41** (1969) 205.

[39] *Probing the Proton's Quark Dynamics in Semi-Inclusive Pion Production at 12 GeV*, PAC-30 E12-06-112 proposal, spokerspersons: H. Avakian, Z-E. Meziani, B. Seitz and K. Joo.

[40] M.E. Christy and P.E. Bosted, arXiv:0712.3731 (2007).

[41] P.E. Bosted and M.E. Christy, Phys. Rev. C **77** (2008) 065206.

[42] *Scaling Study of the L-T Separated Pion Electroproduction Cross Section at 11 GeV*, PAC-32 E12-07-105 proposal, spokespersons: T. Horn and G. Huber.

[43] *Studies of the L-T Separated Kaon Electroproduction Cross Section from 5-11 GeV*, PAC-34 E12-09-011 proposal, spokespersons: T. Horn, G. Huber, and P. Markowitz.

[44] R. Asaturyan *et al.*, Nucl. Instr. and Meth. **A548**, 364 (2005).

[45] M. Contalbrigo, E. Cisbani, P. Rossi, Nucl. Instr. and Meth. Phys. Res., Sect A, Available online October, 2010

[46] A. Afanasev and C. Carlson, Phys. Rev. D **74** (2006) 114027.

[47] A. D. Martin, R. G. Roberts, W. J. Stirling and R. S. Thorne, Eur. Phys. J. **C 35** (2004) 325 [arXiv:hep-ph/0308087].